







# O-GlcNAcylation promotes topoisomerase II $\alpha$ catalytic activity in breast cancer chemoresistance

Yangzhi Liu<sup>1,†</sup>, Kairan Yu<sup>1,†</sup>, Keren Zhang<sup>2,†</sup>, Mingshan Niu<sup>3</sup>, Qiushi Chen<sup>4,5</sup> , Yajie Liu<sup>1</sup>, Lingyan Wang<sup>1</sup>, Nana Zhang<sup>1</sup>, Wenli Li<sup>1</sup> , Xiaomin Zhong<sup>6</sup>, Guohui Li<sup>7</sup> , Sijin Wu<sup>7,\*</sup> , Jianing Zhang<sup>1,\*\*</sup>  & Yubo Liu<sup>1,\*\*\*</sup> 

## Abstract

DNA topoisomerase II $\alpha$  (TOP2A) plays a vital role in replication and cell division by catalytically altering DNA topology. It is a prominent target for anticancer drugs, but clinical efficacy is often compromised due to chemoresistance. In this study, we investigate the role of TOP2A O-GlcNAcylation in breast cancer cells and patient tumor tissues. Our results demonstrate that elevated TOP2A, especially its O-GlcNAcylation, promotes breast cancer malignant progression and resistance to adriamycin (Adm). O-GlcNAcylation at Ser1469 enhances TOP2A chromatin DNA binding and catalytic activity, leading to resistance to Adm in breast cancer cells and xenograft models. Mechanistically, O-GlcNAcylation-modulated interactions between TOP2A and cell cycle regulators influence downstream gene expression and contribute to breast cancer drug resistance. These results reveal a previously unrecognized mechanistic role for TOP2A O-GlcNAcylation in breast cancer chemotherapy resistance and provide support for targeting TOP2A O-GlcNAcylation in cancer therapy.

**Keywords** catalytic activity; chemotherapy resistance; O-GlcNAcylation; TOP2A

**Subject Categories** Cancer; DNA Replication, Recombination & Repair; Post-translational Modifications & Proteolysis

**DOI** 10.15252/embr.202256458 | Received 26 November 2022 | Revised 6 May 2023 | Accepted 12 May 2023 | Published online 30 May 2023

**EMBO Reports (2023) 24: e56458**

## Introduction

Two isoforms of topoisomerase II (TOP2A and TOP2B) are essential enzymes in regulating the homeostasis of DNA topology and cellular

survival during replication, transcription, and cell proliferation (Nitiss, 2009; Pommier *et al*, 2016). TOP2A is associated with cell mitosis and division by catalyzing cleavage/ligation double-strand DNA breaks that disentangle the superhelical and interlinked states of genomic DNA (Pommier *et al*, 2022). Because of its critical role, TOP2A has been identified as a major target for developing antineoplastic chemotherapeutic drugs that hamper its DNA cleavage activity (McClendon & Osheroff, 2007; Chen *et al*, 2015; Hevener *et al*, 2018). These drugs are widely used in the clinic for a variety of both hematological and solid malignancies, including breast cancer (Bailly, 2012). Chemotherapy drug (e.g., adriamycin, Adm) stabilize the covalent TOP2A-DNA cleavage complex and block ligation of the temporary strand breaks, overwhelming cancer cells and causing cell death (Tewey *et al*, 1984; Nitiss, 2009). However, the development of drug resistance is the most common clinically encountered phenomenon that leads to the failure of breast cancer therapy (Coley, 2008; Li *et al*, 2008). Exploration of the mechanisms through which TOP2A resistance occurs has huge implications for improving therapeutic efficacy.

The catalytic activity of TOP2A is modulated by several different mechanisms in mammalian cells (Chen *et al*, 2015; Lotz & Lamour, 2020). Among the multiple folded domains in this evolutionarily conserved enzyme, the C-terminal domain (CTD) with a highly variable amino acid sequence and low complexity structure is thought to influence TOP2A cellular localization and catalytic activity (Dougherty *et al*, 2021). Accumulating evidence shows that the TOP2A CTD plays an important role in regulating TOP2A catalytic activity and cancer therapeutic responsiveness (Linka *et al*, 2007; Kozuki *et al*, 2017; Hoang *et al*, 2020). This region contains a variety of posttranslational modifications (PTMs) that influence TOP2A biological functions or stability (Lotz & Lamour, 2020). The hyperphosphorylation of TOP2A was linked to drug response in

1 School of Life and Pharmaceutical Sciences, Dalian University of Technology, Panjin, China

2 Department of Chemistry, College of Science, Southern University of Science and Technology, Shenzhen, China

3 Blood Diseases Institute, Xuzhou Medical University, Xuzhou, Jiangsu, China

4 Department of Chemistry, The University of Hong Kong, Hong Kong, China

5 Laboratory for Synthetic Chemistry and Chemical Biology Limited, Hong Kong Science Park, Hong Kong, China

6 Department of Oncology, The Affiliated Huaian No. 1 People's Hospital of Nanjing Medical University, Huai'an, China

7 Laboratory of Molecular Modeling and Design, State Key Laboratory of Molecular Reaction Dynamics, Dalian Institute of Chemical Physics, Chinese Academy of Sciences, Dalian, China

\*Corresponding author. Tel: 0411-84379198; E-mail: sijin\_wu@foxmail.com

\*\*Corresponding author. Tel: 0427-2631889; E-mail: jnzhang@dlut.edu.cn

\*\*\*Corresponding author. Tel: 0427-2631413; E-mail: liuyubo@dlut.edu.cn

<sup>†</sup>These authors contributed equally to this work

breast and other cancer cells (Matsumoto *et al*, 1997; Chikamori *et al*, 2003; Gmeiner & van Waardenburg, 2021). Introduction of ubiquitin is another mechanism of chemotherapy resistance, as it not only alters TOP2A biochemical activity but also depletes target levels through proteasome degradation (Guturi *et al*, 2016; Fielding *et al*, 2018). Recently, we discovered that chromatin complexes are prevalently modified by an *O*-linked N-acetylglucosamine moiety (*O*-GlcNAc), which contributes to chemotherapy resistance in cancer cells (Liu *et al*, 2020). This finding implies that glycosylation may be involved in modulating TOP2A activity.

*O*-GlcNAcylation is a monosaccharide modification that occurs on the serine or threonine residues of nuclear and cytoplasmic proteins (Yang & Qian, 2017). Only *O*-GlcNAc transferase (OGT) and *O*-GlcNAcase (OGA) dynamically and reversibly catalyze this PTM. *O*-GlcNAcylation is critical in maintaining chromatin physiological function (Ma *et al*, 2021). Abnormal chromatin-associated *O*-GlcNAc modification can affect chromatin homeostasis, gene transcription, DNA–protein, and protein–protein interactions in various tumors. Topoisomerase I (TOP1) was previously demonstrated as an *O*-GlcNAcylated protein in cell lines and animal models (Noach *et al*, 2007). *O*-GlcNAcylation affects TOP1 DNA relaxation activity and downstream gene expression (Levi *et al*, 2012). However, it is currently unknown whether TOP2A is *O*-GlcNAc-modified, and the mechanism by which interplay between TOP2A and *O*-GlcNAcylation affects breast cancer chemotherapeutic drug resistance remains unclear.

In the current study, we provide evidence that TOP2A is hyper-*O*-GlcNAcylated by OGT at the conserved serine 1469 (S1469) in Adm-resistant breast cancer cells. We further compared biochemical activity between *O*-GlcNAcylated and unmodified TOP2A and revealed that this PTM induces TOP2A catalytic DNA cleavage and decatenation. Meanwhile, *O*-GlcNAcylation enhances the interaction between TOP2A and cell cycle regulators, in turn playing a crucial role in breast cancer progression and Adm resistance *in vitro* and *in vivo*. Our results provide novel mechanistic insights into TOP2A-mediated breast cancer malignant progression and provide potential therapeutic opportunities for reversing breast cancer drug resistance by blocking TOP2A *O*-GlcNAcylation.

## Results

### TOP2A and cellular *O*-GlcNAcylation are significantly upregulated in breast cancer

To investigate the clinical relevance of TOP2A in breast cancer, we examined *TOP2A* transcriptional expression in The Cancer Genome Atlas (TCGA) database (Chang *et al*, 2013). The results revealed that *TOP2A* was significantly upregulated in breast cancer tissues ( $n = 1,072$ ) compared with normal tissues ( $n = 99$ ,  $P < 0.0001$ , Fig 1A). *TOP2A* mRNA levels in clinical cancer tissue samples were also significantly higher than those in their paired adjacent normal tissues ( $n = 94$ ,  $P < 0.0001$ , Fig 1B and C). Multivariate analysis further showed that high *TOP2A* mRNA levels were correlated with advanced tumor stage (Fig 1D) and clinical T classification in breast cancer patients (Appendix Table S1). Correspondingly, overall survival in patients with higher *TOP2A* expression levels was significantly worse compared with patients with lower *TOP2A* expression

( $P = 1.2e-5$ , Fig 1E). Similar results were found in two other independent breast cancer cohorts (GSE48390 (Huang *et al*, 2013) and GSE3494 (Miller *et al*, 2005), Fig EV1), indicating the role of TOP2A in breast cancer malignancy.

Our previous study revealed that cellular protein *O*-GlcNAcylation is an important regulator of cell death thresholds to chemotherapeutic drugs in cancer cells (Liu *et al*, 2018, 2020). To obtain a comprehensive understanding of the relationship between TOP2A and cellular *O*-GlcNAcylation, tissue microarrays of human breast cancer were evaluated by immunohistochemistry (IHC) analysis (Appendix Fig S1). Representative images indicated higher expression of TOP2A and cellular *O*-GlcNAcylation in breast cancer tissues compared with adjacent normal tissues (Fig 1F). Our results also showed that TOP2A and cellular *O*-GlcNAcylation levels increased correspondingly with the aggressiveness of the disease (Fig 1G and H). The clinical and pathologic features are presented in Appendix Tables S2 and S3. In addition, a positive correlation was found between TOP2A and cellular *O*-GlcNAcylation in breast cancer tissues (Spearman correlation coefficient  $r = 0.2717$ ,  $P = 0.0009$ , Fig 1I), indicating that the interplay between TOP2A and *O*-GlcNAcylation might be an important point in breast cancer malignancy. In summary, these data validated that increased TOP2A and cellular *O*-GlcNAcylation were associated with poor clinical outcomes in breast cancer.

### TOP2A is hyper-*O*-GlcNAcylated in chemotherapy-resistant breast cancer cells

Next, we revealed that TOP2A expression was not much different in adriamycin (Adm)-resistant breast cancer cell lines (MDA-MB-231, MCF-7/ADR) compared with Adm-sensitive breast cancer cells (MCF-7, T47D, Fig 2A–C), indicating the likelihood of other regulatory mechanisms involving TOP2A-related drug resistance. An increase in cellular *O*-GlcNAcylation was found in Adm-resistant cells with elevated cell survival and colony formation frequency under Adm treatment. However, no clear correlation was identified between OGT levels and cellular response to Adm. In Adm-resistant MDA-MB-231 and MCF-7/ADR cells, inhibition of *O*-GlcNAcylation with L01 (a cell-permeable OGT inhibitor developed in our previous research; Liu *et al*, 2017) or TOP2A shRNA-transfection (shTOP2A) did not affect cell viability alone, while co-treatment with L01/shTOP2A and Adm significantly reduced the cell viability (Fig 2D and E; Appendix Fig S2). Regardless of the *O*-GlcNAcylation levels, the expression levels of multidrug resistance-related ABC transporter P-glycoprotein (P-gp) remained unchanged in MDA-MB-231 and MCF-7/ADR cells. These results suggested that an impact on both TOP2A and *O*-GlcNAcylation protects breast cancer cells from Adm-induced cell death in a P-gp-independent manner.

In our previous report, TOP2A was identified as a candidate *O*-GlcNAc-modified protein. Quantitative mass spectrometry showed that the chromatin association of TOP2A was increased (fold change  $> 2$ ,  $P < 0.05$ ) in Adm-resistant MCF-7/ADR cells compared with parental MCF-7 cells (Appendix Fig S3; Liu *et al*, 2020), suggesting that the *O*-GlcNAcylation of TOP2A might participate in chemotherapy resistance. To further verify this result, we confirmed that endogenous TOP2A was *O*-GlcNAcylated via multiple methods, including co-immunoprecipitation, succinylated wheat germ agglutinin lectin (sWGA, lectin specifically recognizes the *O*-GlcNAc

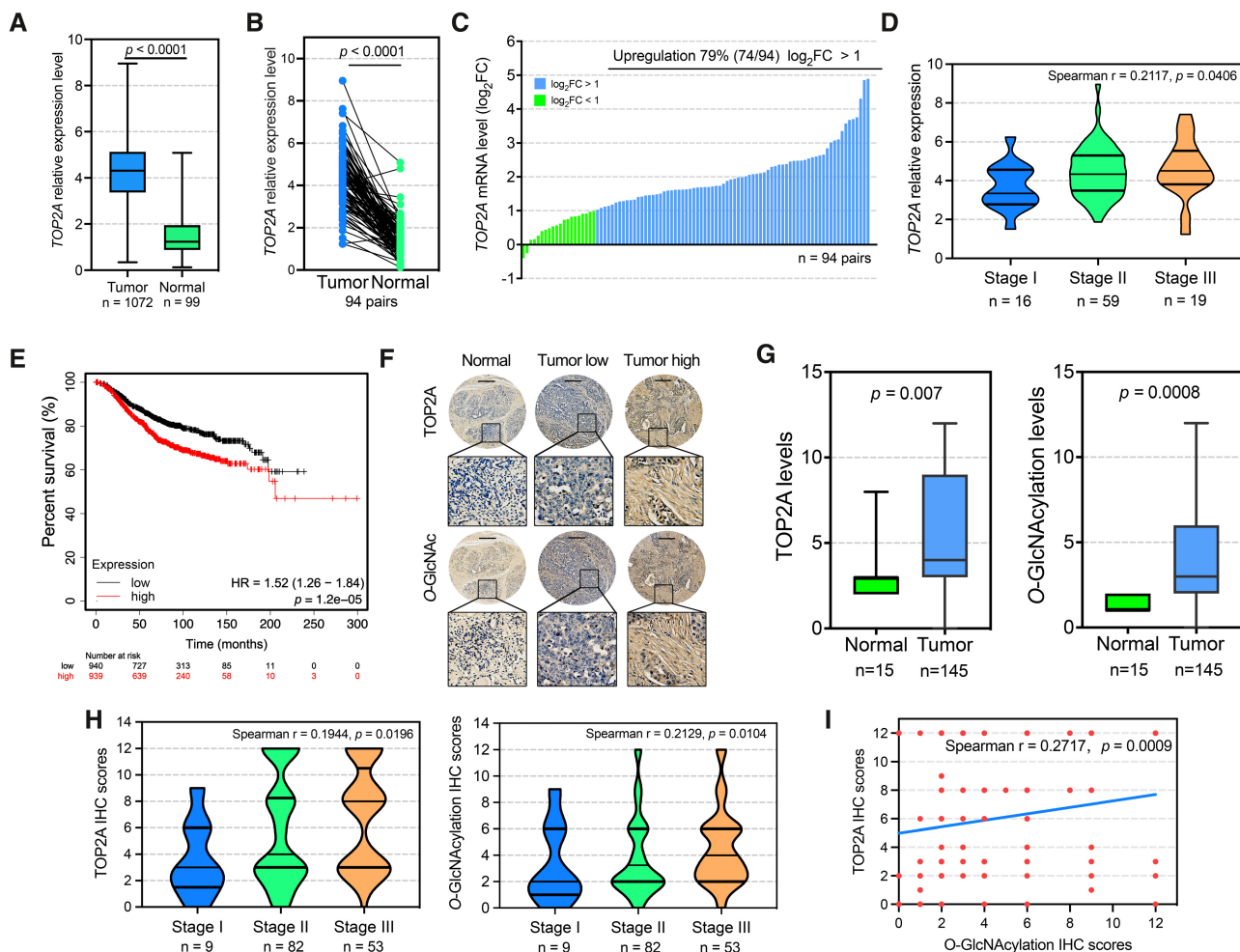


**Figure 1. Role of TOP2A is linked to cellular O-GlcNAcylation in breast cancer patients with poor clinical prognosis.**

- A The mRNA expression of *TOP2A* in breast tumor tissue ( $n = 1,072$  biological replicates) and normal breast tissue samples ( $n = 99$  biological replicates) according to TCGA database. The box plots show the medians (black lines), 25<sup>th</sup> and 75<sup>th</sup> percentiles (boundaries), and minimum/maximum values (whiskers). Unpaired t-test was used for statistical comparison. The *P*-value is indicated.
- B, C *TOP2A* mRNA levels were compared between 94 pairs (biological replicates) of breast tumor tissues and their paired adjacent normal tissues from TCGA database. Wilcoxon matched-pair signed-rank test was used. The blue bar represents  $\log_2FC > 1$ . The green bar represents that  $\log_2FC < 1$ . Paired *t*-test was used for statistical comparison. The *P*-value is indicated. FC, fold change (tumor/normal).
- D Spearman correlation coefficient of *TOP2A* mRNA expression among different progression stages from 94 pairs (biological replicates) of TCGA breast tumor tissues. The violin plots show the 25<sup>th</sup>, 50<sup>th</sup>, and 75<sup>th</sup> percentiles. The Spearman correlation *P*-value is indicated.
- E In TCGA breast cancer tissues, the samples with higher *TOP2A* mRNA levels had shorter overall survival times than those with lower *TOP2A* mRNA levels ( $n = 1879$  biological replicates). Patients with *TOP2A* expression greater than the median are indicated by the red line, and patients with *TOP2A* expression below the median are indicated by the black line. HR, hazard ratio. Statistical analysis was performed by the log-rank test. The *P*-values are indicated.
- F Representative IHC staining of *TOP2A* and cellular O-GlcNAcylation on a tissue microarray containing 145 breast tumor and 15 adjacent samples. Histological scoring was based on the positive percentages and intensity of stained cells. The micrograph scale bar represents 250  $\mu$ m.
- G *TOP2A* and cellular O-GlcNAcylation expression levels were compared between breast tumor tissues ( $n = 145$  biological replicates) and normal adjacent tissues ( $n = 15$  biological replicates). The box plots show the medians (black lines), 25<sup>th</sup> and 75<sup>th</sup> percentiles (boundaries), and minimum/maximum values (whiskers). Unpaired *t*-test was used for statistical comparison. The *P*-value is indicated.
- H Spearman correlation coefficient of *TOP2A* and cellular O-GlcNAc expression among different progression stages from tissue microarray. The violin plots show the 25<sup>th</sup>, 50<sup>th</sup>, and 75<sup>th</sup> percentiles. One sample (Stage 0) was excluded. The Spearman correlation *P*-value is indicated.
- I Correction analysis of *TOP2A* and O-GlcNAcylation expression levels in 145 breast tumor tissues. Spearman correlation test was used. The *P*-value is indicated.

moiety) pull-down, and the GalT1(Y289L)-mediated chemical enzymatic method (Fig 2F–H). Remarkably, Adm-resistant cells showed higher levels of TOP2A O-GlcNAcylation and TOP2A-OGT/HCFC1 (an important OGT partner; Daou et al, 2011) interactions compared with Adm-sensitive cells. Since one of the primary therapeutic

mechanisms of Adm is the stabilization of TOP2-DNA covalent complexes (TOP2Acc), we further elucidated the relationship between Adm-induced TOP2Acc and TOP2A O-GlcNAcylation-related Adm resistance by TOP2A band depletion assays. As shown in Fig EV2A, Adm-trapped TOP2A into TOP2Acc in Adm-sensitive MCF-7 cells.

On the contrary, the amount of Adm-trapped TOP2Acc was greatly reduced in Adm-resistant MDA-MB-231 and MCF-7/ADR cells, indicating that the Adm resistance in these cells is at least in part due to reduced TOP2Acc. Moreover, both OGT knockdown and the inhibition of cellular O-GlcNAcylation with L01 restrained TOP2A

modification and enhanced DNA damage marker  $\gamma$ -H2AX expression in MDA-MB-231 and MCF-7/ADR cells (Figs 2I and EV2B). Collectively, these data demonstrated that TOP2A is a novel O-GlcNAc-modified protein that its hyperglycosylation contributes to chemotherapy resistance in breast cancer cells.

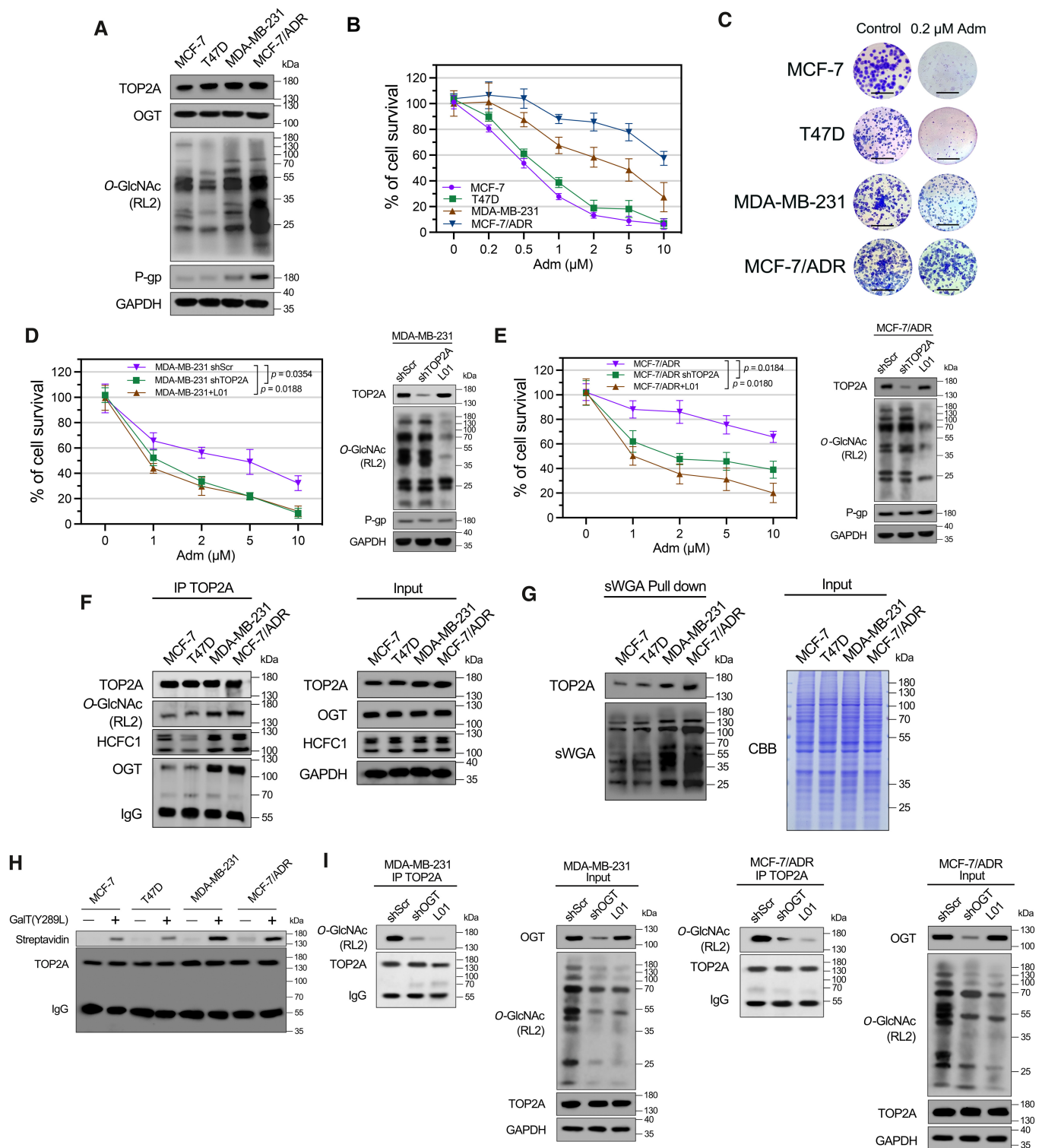


Figure 2.

**Figure 2. Hyper-O-GlcNAcylation of TOP2A increases drug resistance in breast cancer cells.**

- A Expression of TOP2A, OGT, P-gp, and cellular O-GlcNAcylation in Adm-sensitive and Adm-resistant breast cancer cell lines was analyzed by Western blot analysis.
- B Breast cancer cells were treated with increasing doses of Adm alone for 48 h, and the cell viability was assessed using CCK-8 assay.  $n = 3$  biological replicates. The data are presented as means  $\pm$  SD.
- C Colony formation assays were performed in breast cancer cells exposed to 0.2  $\mu$ M Adm. The micrograph scale bar represents 5 mm.
- D, E MDA-MB-231 or MCF-7/ADR cells were transfected with TOP2A shRNA (shTOP2A) or treated with 50  $\mu$ M L01 and then incubated with the indicated doses of Adm for 48 h. Cell viability was assessed with a CCK-8 assay. Protein expression was analyzed by Western blot. shScr, scrambled shRNA.  $n = 3$  biological replicates. Paired t-test was used for statistical comparison.  $P$ -value was indicated. The data are presented as means  $\pm$  SD.
- F TOP2A co-IP was performed, and the immunoprecipitated fractions were analyzed by Western blot for the indicated proteins.
- G sWGA lectin pull-down was performed, and precipitated fractions were analyzed by Western blot and lectin blot. CBB, Coomassie Brilliant Blue staining.
- H The O-GlcNAc enzymatic labeling system was employed to confirm the O-GlcNAcylation of endogenous TOP2A in breast cancer cells. TOP2A IP was performed, and immunoprecipitated fractions were incubated with Y289L GalT1. Streptavidin beads were used to capture O-GlcNAc proteins. An anti-TOP2A antibody was used for immunoblotting.
- I MDA-MB-231 or MCF-7/ADR cells were transfected with OGT shRNA (shOGT) or treated with 50  $\mu$ M L01 for 48 h. TOP2A co-IP was performed, and the immunoprecipitated fractions were analyzed by Western blot for the indicated proteins.

**OGT promotes TOP2A O-GlcNAcylation at S1469, which strengthens TOP2A chromatin binding.**

The online server YinOYang (v1.2) was used to predict potential TOP2A O-GlcNAcylation site(s), and the majority were predicted within the CTD (Fig 3A). We then prepared three truncated TOP2A variants (TOP2A-A to TOP2A-C, Fig 3B). HEK-293T cell-derived OGT and these prokaryotically expressed recombinant His-tagged TOP2A fragments were employed in an *in vitro* glycosylation assay. Only TOP2A-C (CTD) could interact with OGT and be further modified (Fig 3C). Similar result was found in OGT overexpressed eukaryotic system (Appendix Fig S4). EThcD-MS/MS analysis was performed to precisely map the O-GlcNAcylation site(s) on TOP2A-C. The results revealed that O-GlcNAcylation occurs on S1469 (within TOP2A nuclear localization signal sequence, NLS, amino acids 1,454–1,497 (Kozuki *et al*, 2017), Fig 3B) in the peptide (RKPSTSDSDSNFEK) spanning residues 1,466–1,480 (Fig 3D). Multiple-sequence alignment revealed that the S1469 residue is highly conserved across species (Fig 3E). Next, we generated an HA-tagged TOP2A construct with S1469 mutated to alanine (TOP2A-S1469A). In Adm-resistant MDA-MB-231 and MCF-7/ADR cells stably transfected with wild-type (TOP2A-WT) or TOP2A-S1469A constructs, the O-GlcNAcylation levels were clearly reduced in mutant compared with wild-type TOP2A. In the presence of the O-GlcNAcylation agonist PugNAc (an OGA inhibitor), no visible TOP2A-S1469A O-GlcNAcylation increase was observed. In contrast, L01 markedly decreased the level of O-GlcNAcylation in TOP2A-WT, supporting the notion that the majority of TOP2A O-GlcNAcylation occurs on S1469 (Fig 3F).

Because O-GlcNAcylation often competes with phosphorylation in many biological processes (Yang & Qian, 2017), we wondered whether the phosphorylation of TOP2A is affected by different O-GlcNAcylation states. Experimental results showed that the phosphorylation level (overall serine and threonine) of TOP2A-S1469A was clearly attenuated compared with that of TOP2A-WT, suggesting an interplay between O-GlcNAcylation and phosphorylation of TOP2A (Fig 3G). Because the O-GlcNAcylation site located in the NLS of this enzyme, we next investigated the role of O-GlcNAcylation in recruiting TOP2A to chromatin in nucleus. Even though similar expression levels were found for the two recombinant forms of TOP2A, TOP2A-S1469A showed significantly less chromatin binding capacity and more cytoplasm localization compared with hyper-O-GlcNAcylation TOP2A-WT in MDA-MB-231 and

MCF-7/ADR cells, indicating that O-GlcNAcylation on S1469 affects TOP2A subcellular localization. Furthermore, the suppression of TOP2A-WT glycosylation by the OGT inhibitor decreased chromatin-associated TOP2A and elevated cytoplasm localization of this enzyme, whereas the OGA inhibitor PugNAc showed the opposite effect (Fig 3H and I). We also observed that more TOP2A-S1469A was diffused in the cytosol in MCF-7/ADR cells than in MDA-MB-231 cells. In Fig 3G, threonine phosphorylation level of TOP2A-S1469A in MCF-7/ADR cells was lower compared with that of MDA-MB-231, indicating the interplay between O-GlcNAcylation and phosphorylation may also participate in nuclear localization of TOP2A. We next tested whether site-specific O-GlcNAcylation reflects the formation of Adm-induced TOP2Acc. O-GlcNAcylation site mutation (TOP2A-S1469A) or L01 treatment increased the amount of TOP2A covalently trapped on DNA compared with wild-type glycosylated TOP2A-WT in Adm-resistant breast cancer cells, suggesting that TOP2A O-GlcNAcylation impeded the formation of Adm-induced TOP2Acc and reduced cytotoxicity (Fig EV2C). Together, these results suggest that the abundance of chromatin-bound TOP2A is modulated by O-GlcNAcylation at S1469 and this modification can further affect the biological function of this enzyme.

**O-GlcNAcylation of TOP2A promotes catalytic activity**

To further assess whether TOP2A CTD O-GlcNAcylation affects its biochemical function, the endogenous enzyme (purified from MCF-7/ADR cells) was first shown to retain overall catalytic activity *in vitro* and to catalyze supercoiled plasmid DNA cleavage in a concentration- and time-dependent manner (Fig EV3). Hyper-O-GlcNAcylation TOP2A from Adm-resistant breast cancer cells displayed greater DNA cleavage efficiency compared with less O-GlcNAcylation TOP2A from Adm-sensitive cells (Fig 4A). Following treatment with PugNAc, the DNA cleavage activity of MCF-7-extracted TOP2A was enhanced. In contrast, the linear state plasmid was attenuated when TOP2A O-GlcNAcylation levels were reduced by L01 in MDA-MB-231 and MCF-7/ADR cells. This was further confirmed by using a commercially available recombinant full-length human TOP2A (Fig 4B) in an *in vitro* glycosylation assay. Then, we examined the effect of O-GlcNAcylation at S1469 on TOP2A catalytic activity. HEK-293T cells stably overexpressing OGT were transfected with HA-tagged TOP2A-WT or TOP2A-S1469A expression plasmids. As shown in Fig 4C, loss of O-GlcNAcylation led to a noticeable

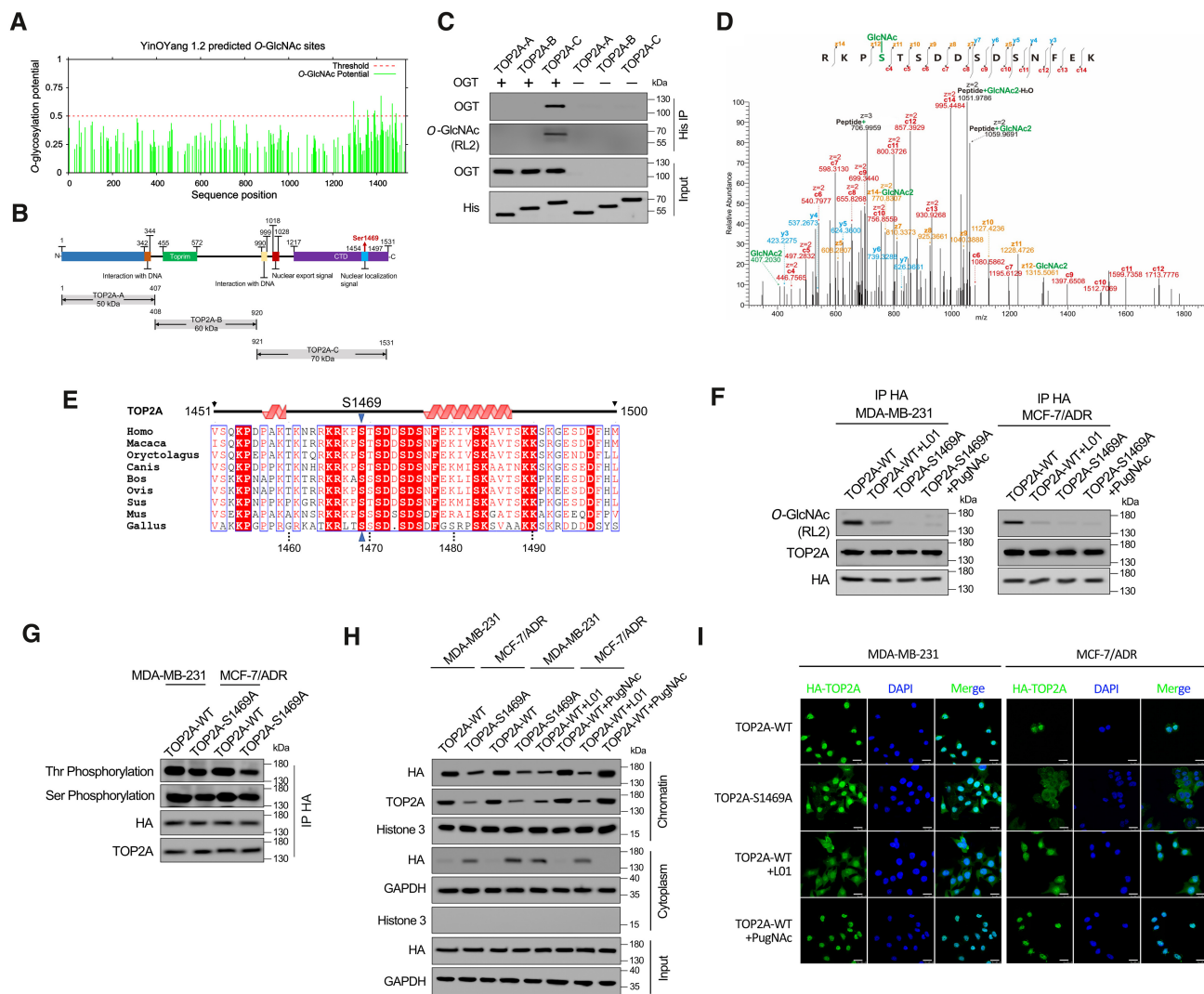


**Figure 3. O-GlcNAcylation at S1469 enhances TOP2A chromatin binding.**

- A** O-GlcNAc sites of human TOP2A predicted using the YinOYang 1.2. The potential O-GlcNAcylated Ser/Thr residues and the threshold for O-GlcNAcylation potential were indicated.
- B** Schematic diagram of key domains in TOP2A. Three truncated variants of TOP2A (TOP2A-A to C) fused with 6 × His-tag were generated according to its key domains.
- C** *In vitro* glycosylation assay was performed using recombinant His-tagged truncated variants of TOP2A and purified OGT. The reaction product was detected by co-immunoprecipitation (co-IP) and Western blot.
- D** ETHcD-MS/MS spectrum of the TOP2A CTD peptide with the O-GlcNAcylation site located on S1469. The matched fragment ions are labeled.
- E** Alignment of TOP2A CTD sequence among different species.
- F** MDA-MB-231 and MCF-7/ADR cells which stable transfected with TOP2A-WT or TOP2A-S1469A were treated with 50 μM L01 or PugNac for 48 h. HA-tag co-IP was performed, and the immunoprecipitated fractions were analyzed by Western blot for the indicated proteins.
- G** HA-tag co-IP was performed in MDA-MB-231 and MCF-7/ADR cells which stable transfected with TOP2A-WT or TOP2A-S1469A. Overall threonine (Thr) and serine (Ser) phosphorylation states of TOP2A were analyzed by Western blot.
- H** Western blots showing the chromatin binding and subcellular localization of TOP2A-WT or TOP2A-S1469A with 50 μM L01 or PugNac treatment in breast cancer cells.
- I** Fluorescent staining results showing nuclear localization dependence of TOP2A on O-GlcNAcylation in MDA-MB-231 and MCF-7/ADR cells. The micrograph scale bar represents 25 μm.

decrease in cleavage activity. Further experiments revealed that the suppression of TOP2A-WT glycosylation by L01 reduced enzymatic activity, but PugNac treatment could not increase the catalytic activity of TOP2A-S1469A. Similar results were obtained using TOP2A-WT and TOP2A-S1469A purified from Adm-resistant breast cancer

cells (Fig 4D). These findings suggest that O-GlcNAcylation is involved in regulating the DNA cleavage activity of TOP2A.

Because decatenation is another important function of TOP2A catalytic activity (Nitiss, 2009), the ability to unlink catenated DNA circles was measured. Decatenation assays using catenated

kinetoplast DNA (kDNA) minicircles showed that hyper-*O*-GlcNAcylated TOP2A appears to decatenate fairly efficiently, in contrast to TOP2A with low *O*-GlcNAcylation (Figs 4E and F, and EV4).

Moreover, with multiple structural modeling and simulation methods, we found that the *O*-GlcNAcylated TOP2A CTD structure could interact with DNA more effectively. The interaction network

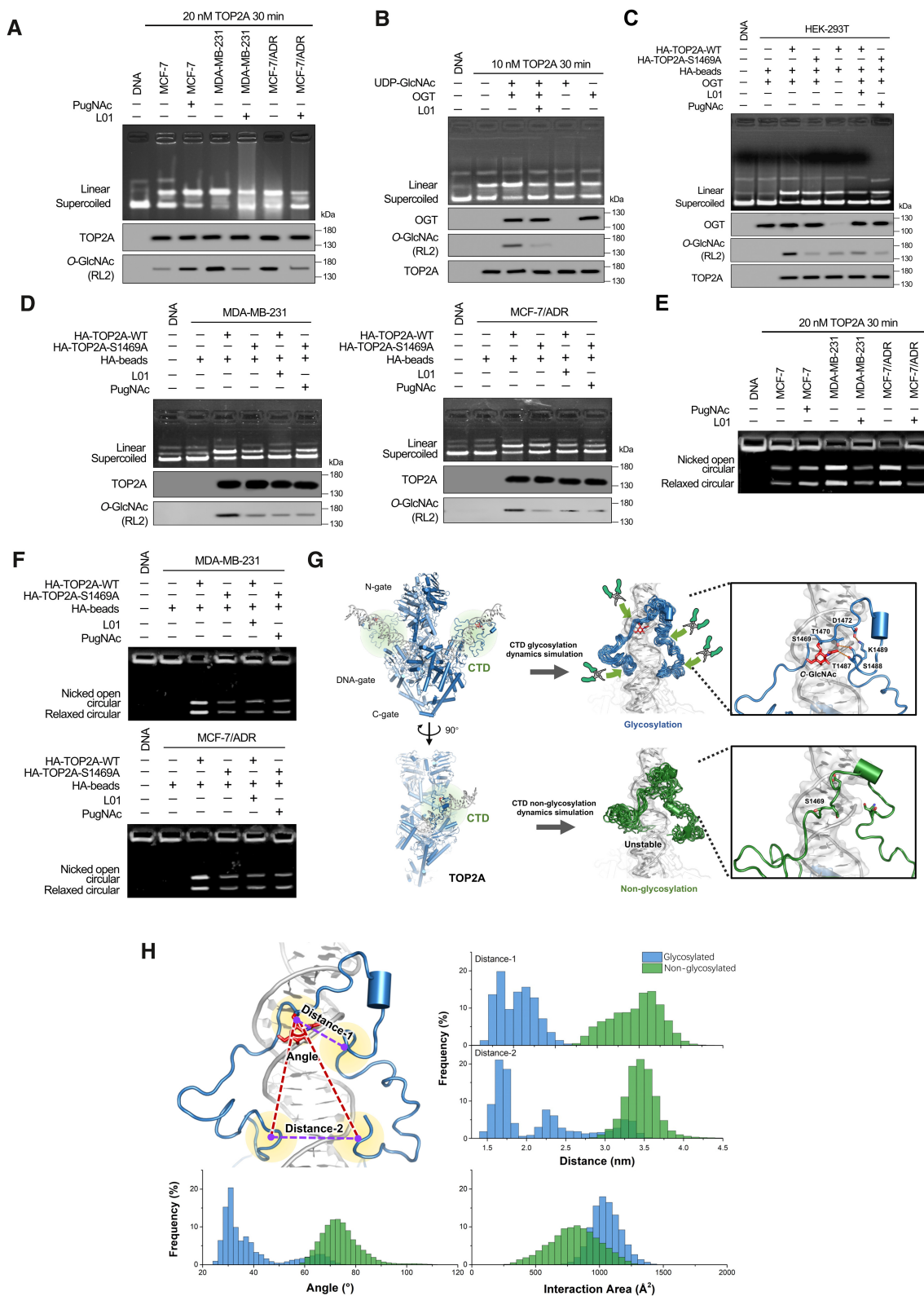


Figure 4.

**Figure 4. O-GlcNAcylation enhances TOP2A enzymatic activity.**

- A DNA cleavage assays were performed using TOP2A extracted (20 nM, reaction for 30 min) from breast cancer cells with 50  $\mu$ M L01 or PugNac treatment (48 h). Supercoiled pBR322 plasmid DNA was used as the TOP2A substrate. TOP2A O-GlcNAcylation status was detected by IP.
- B 10 nM commercially available recombinant full-length human TOP2A was O-GlcNAcylation by an *in vitro* reaction (with or without 50  $\mu$ M L01, reaction for 30 min). The reaction product was then used for DNA cleavage assays and co-IP. The immunoprecipitated fractions were analyzed by Western blot.
- C, D DNA cleavage assays were performed using TOP2A extracted from OGT stably overexpressed HEK-293T cells (C) or breast cancer cells (D). These cells were stably transfected with HA-tagged TOP2A-WT or TOP2A-S1469A expression plasmids and treated with 50  $\mu$ M L01 or PugNac for 48 h. TOP2A-WT or TOP2A-S1469A (20 nM) was immunoprecipitated using anti-HA magnetic beads from breast cancer cells.
- E kDNA decatenation assays were measured using TOP2A extracted (20 nM, reaction for 30 min) from breast cancer cells with 50  $\mu$ M L01 or PugNac treatment (48 h).
- F kDNA decatenation assays were performed using TOP2A extracted from TOP2A-WT or TOP2A-S1469A overexpressed breast cancer cells with 50  $\mu$ M L01 or PugNac treatment (48 h). TOP2A-WT or TOP2A-S1469A (20 nM) was immunoprecipitated using anti-HA magnetic beads from breast cancer cells.
- G Left: Two views of the overall model structure of TOP2A (N-gate, DNA-gate, C-gate from Cryo-EM structure 6ZY8, and CTD structure refined from AlphaFold2 modeling structure with MD simulation), with the substrate DNA helix. Middle: The superposition of CTD structures from the cluster results of glycosylated (blue) and nonglycosylated (green) CTD-DNA systems simulation trajectories. The red stick is the O-GlcNAc group on S1469. Right: The interaction network around O-GlcNAc moiety and S1469, act as a pivot point for the tight association with DNA by the N- and C-terminal loops of CTD, which like two arms of a pincher.
- H The frequency of some crucial variants from 1  $\mu$ s MD simulation trajectories for glycosylated (blue) and nonglycosylated (green) CTD-DNA complex systems, which could describe the difference between these two systems. Distance-1: center of mass distance between S1469 and 1487-TSK-1489. Distance-2: center of mass distance between 1441-TKR-1443 and 1510-AKS-1512. Angle: the angle is formed with the center of mass of S1469 as the vertex, and two vectors from the vertex to the center of mass of 1441-TKR-1443 and 1510-AKS-1512 as the edges. Interaction area: area of the interaction between CTD and DNA.

formed among the O-GlcNAc moiety and the adjacent residues, for example, T1470, D1472, T1487, S1488, and K1489, provided stable support among the large disordered region of the TOP2A CTD, which is beneficial for the stability and tightness of the interaction between the CTD and DNA (Figs 4G and H, and EV5A–D). Taken together, the present data establish that S1469 O-GlcNAcylation has a critical role in promoting the catalytic activity of TOP2A.

#### O-GlcNAcylation-modulated interactions between TOP2A and cell cycle regulators contribute to breast cancer cell drug resistance.

To explore the function of TOP2A O-GlcNAcylation in Adm resistance, cell proliferation and cell cycle assays were performed. Colony formation assays were performed with MCF-7 and MCF-7/ADR cells overexpressing TOP2A-WT or TOP2A-S1469A and treated with Adm for 48 h. The colony formation rate was higher in the TOP2A-WT group and lower in the TOP2A-S1469A group after Adm treatment, affirming that TOP2A glycosylation promoted Adm resistance in breast cancer cells (Fig 5A). We then investigated the effects of TOP2A O-GlcNAcylation on cell cycle progression. Of note, the proportion of cells arrested in S phase by Adm treatment was significantly lower in TOP2A-WT-overexpressing MCF-7 and MCF-7/ADR cells compared with TOP2A-S1469A-overexpressing cells (Fig 5B and C), indicating that TOP2A O-GlcNAcylation at S1469 promotes cell cycle progression.

TOP2A activity can be regulated by interacting with multiple cell cycle regulators (Kang *et al.*, 2015; Jin *et al.*, 2021; Zhu *et al.*, 2021). In the present study, O-GlcNAcylation site mutation or L01 treatment decreased the interaction of TOP2A with the cell cycle activators CDK1 and UPF1, whereas the TOP2A-PTEN dimer was increased in Adm-resistant breast cancer cells (Fig 5D). As a result, hyper TOP2A O-GlcNAcylation in breast cancer cells resulted in higher levels of the downstream cell cycle-related proteins cyclin A2, cyclin D1, and phospho-Rb (S807/811) and lower levels of the cyclin-dependent inhibitors p27 and p57. O-GlcNAcylation inhibition had the opposite effect, suggesting a function of TOP2A O-GlcNAcylation in regulating cell cycle-related protein expression (Fig 5E). Together, these results demonstrated that O-GlcNAcylation modulates the interactions between TOP2A and cell cycle regulators and then activates downstream gene expression, resulting in breast cancer cell Adm resistance.

#### TOP2A O-GlcNAcylation is critical for mediating resistance to Adm

To test whether O-GlcNAcylation could impact Adm-mediated TOP2A inhibition, we examined TOP2A catalytic activity in the presence of Adm. Adm showed no inhibition of TOP2A-WT-catalyzed plasmid DNA cleavage or kDNA decatenation *in vitro* (Fig 6A and B). In contrast, reduction of O-GlcNAcylation by site mutation increased the ability of Adm to inhibit TOP2A. These data support the idea that O-GlcNAcylation of TOP2A prevents Adm from inhibiting catalytic activity. Meanwhile, we noticed an additional 20–30% cell survival, which increased with the duration of TOP2A-WT expression, compared with TOP2A-S1469A expression in drug-sensitive MCF-7 cells (Fig 6C). Similar results were observed in Adm-resistant MDA-MB-231 and MCF-7/ADR cells (Fig 6D and E). From these results, we confirmed that it is TOP2A O-GlcNAcylation but not the TOP2A expression itself protects cells from Adm-induced cell death. Furthermore, five breast cancer patient tumor tissues were examined for TOP2A O-GlcNAcylation. Even though TOP2A expression was similar, chemotherapy-resistant or relapsed patient samples (no. 3–5) contained higher levels of O-GlcNAc-modified TOP2A and TOP2A-OGT/HCF1 interaction compared with sensitive patient samples (no. 1–2, patients' main characteristics are listed in Appendix Table S4). Notably, the interaction between cell cycle activators and TOP2A was increased in resistant samples compared with sensitive samples, and the downstream cell cycle-related gene expression had corresponding changes (Fig 6F). Taken together, these results suggest that TOP2A activation by O-GlcNAcylation may be a common mechanism through which cancer cells antagonize chemotherapy-induced cell death and that this mechanism is at least partially mediated by affecting TOP2A interaction with DNA and other regulators.

#### Blocking TOP2A O-GlcNAcylation improves the therapeutic efficacy of Adm in a xenograft mouse model.

To evaluate the role of TOP2A O-GlcNAcylation in regulating the tumorigenic capacity of breast cancer cells and sensitivity to Adm treatment *in vivo*, breast cancer cells stably transfected with



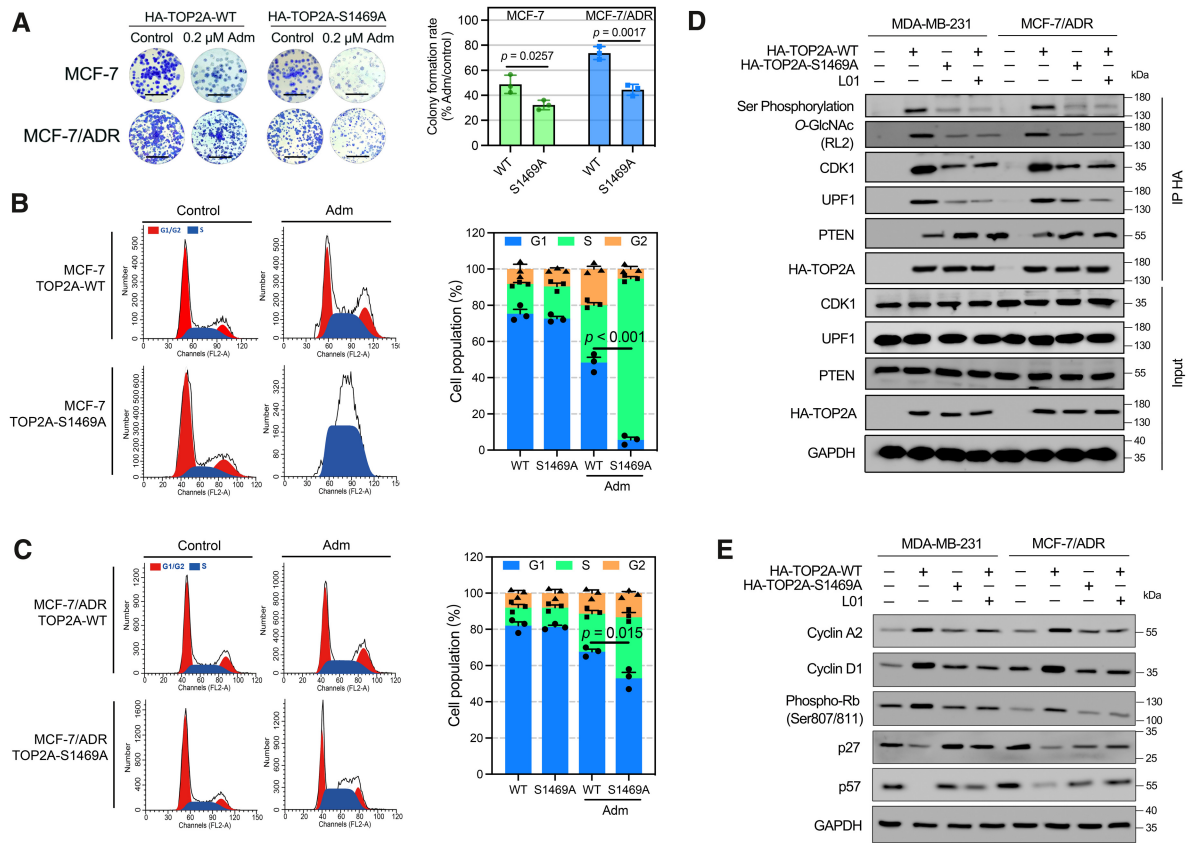


**Figure 5. TOP2A O-GlcNAcylation accelerates breast cancer cell cycle progression.**

- A** Colony formation assays were performed in TOP2A-WT or TOP2A-S1469A stably expressed MCF-7 and MCF-7/ADR cells. Cells were exposed to 0.2  $\mu$ M Adm during the assays. The micrograph scale bar represents 5 mm. The colony formation rate was calculated.  $n = 3$  biological replicates. Unpaired t-test was used for statistical comparison.  $P$ -value was indicated. The data are presented as means  $\pm$  SD.
- B, C** Flow cytometry was employed to identify the percentage of cells in G1, S, and G2 phases. TOP2A-WT or TOP2A-S1469A stably expressed MCF-7 and MCF-7/ADR cells were treated with Adm (0.5  $\mu$ M for MCF-7 cells, 2  $\mu$ M for MCF-7/ADR cells) for 24 h.  $n = 3$  biological replicates. Unpaired t-test was used for statistical comparison.  $P$ -value was indicated. The data are presented as means  $\pm$  SD.
- D** Breast cancer cells expressing TOP2A-WT or TOP2A-S1469A were immunoprecipitated with anti-HA magnetic beads, and the interaction between TOP2A and cell cycle regulators was analyzed. Cells were treated with 50  $\mu$ M L01 for 48 h before immunoprecipitation.
- E** Cell cycle-related protein expression was measured using Western blot in Breast cancer cells expressing TOP2A-WT or TOP2A-S1469A. Cells were treated with 50  $\mu$ M L01 for 48 h before immunoprecipitation.

scrambled shRNA (shScr) or TOP2A shRNA (shTOP2A) were further transfected with TOP2A-WT or TOP2A-S1469A constructs and subcutaneously injected into female athymic nude mice. Even though knockdown of TOP2A inhibited the tumor proliferation, the mice bearing MDA-MB-231 shTOP2A + S1469A cells showed much slower tumor growth than MDA-MB-231 shTOP2A + WT-injected group (Fig 6G). We also observed that L01 treatment significantly decreased tumor volumes for both wild-type MDA-MB-231 (Appendix Fig S5A) and shTOP2A + WT xenografts (Fig 6G), indicating the important role of TOP2A O-GlcNAcylation but not the expression itself in breast cancer malignancy. Furthermore, a mouse model with MCF-7/ADR-derived cells was established. The mice received administration of Adm (4 mg/kg) every 7 days. The average tumor volume was reduced in the presence of TOP2A silencing or TOP2A-S1469A overexpression, and this reduction was reversed when TOP2A silencing was combined with TOP2A-WT overexpression (Fig 6H). We also revealed that L01 treatment decreased tumor

volumes for MCF-7/ADR xenografts (Appendix Fig S5B). Notably, the combination of O-GlcNAc inhibition by L01 and Adm treatment resulted in much more pronounced suppression of tumor growth in mice bearing MCF-7/ADR shTOP2A + WT cells compared with Adm treatment alone. Kaplan–Meier survival curves showed that mice injected with MCF-7/ADR shTOP2A, MCF-7/ADR shTOP2A + S1469A or MCF-7/ADR shTOP2A + WT + L01 all survived within an experimental period of 30 days (Fig 6I). In contrast, mice that received MCF-7/ADR shRNA or MCF-7/ADR shTOP2A + WT cells only had a significantly shorter median survival time (approximately 22 days). In line with the impaired tumor growth, the interaction between TOP2A and cell cycle activators was decreased in TOP2A O-GlcNAcylation-inhibited tumor tissues (Fig 6J). Corresponding results were obtained by IHC analysis of Cyclin A2 and p27 in tumor tissues (Fig 6K). These data again demonstrate that O-GlcNAcylation at S1469 can promote TOP2A activity and further contribute to tumor growth and drug resistance in breast cancer.

## Discussion

Although there are numerous complicated mechanisms involved in breast cancer drug resistance (Vasan *et al*, 2019), including the inactivation of drug targets, the enhancement of drug efflux by overexpressing P-gp, and the activation of pro-survival pathways, the precise regulatory processes of drug tolerance in breast cancer remain unclear. In the present study, we uncovered the functional and mechanistic role of TOP2A O-GlcNAcylation in breast cancer progression and response to the chemotherapeutic drug Adm. We discovered that both of TOP2A and cellular O-GlcNAcylation

expression were increased in breast cancer tissues at the transcriptional and protein levels, and this was accompanied by malignant progression. As a novel PTM on TOP2A (S1469), O-GlcNAcylation was demonstrated to elevate TOP2A catalytic activity, which is crucial for drug resistance, by intensifying the binding with DNA. These data add a new layer of complexity to the PTM code in modulating TOP2A biochemical functions, which enables increased chemotherapy cell death thresholds in breast cancer.

Our data showed that the TOP2A-OGT interaction was enhanced in drug-resistant breast cells/patient samples compared with the drug-sensitive ones. The underlying molecular mechanism can be

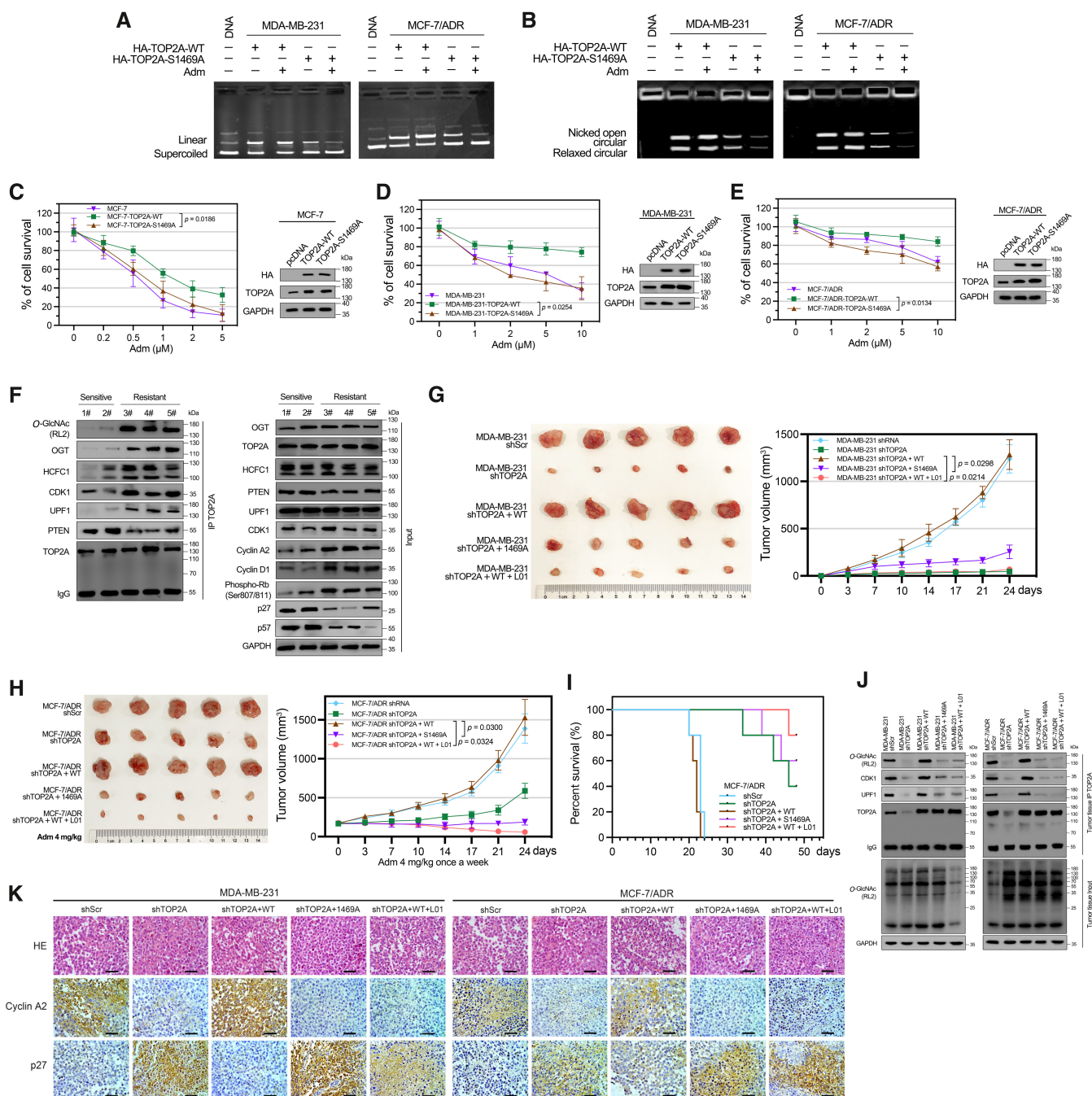


Figure 6.

**Figure 6. O-GlcNAcylation contributes to Adm resistance *in vitro* and *in vivo*.**

- A, B O-GlcNAcylation attenuated Adm-induced inhibition of TOP2A catalytic activity in DNA cleavage (A) and kDNA decatenation assays (B). TOP2A-WT or TOP2A-S1469A (20 nM) was immunoprecipitated using anti-HA magnetic beads from breast cancer cells. 200  $\mu$ M Adm was added during the reaction (30 min).
- C–E TOP2A-WT or TOP2A-S1469A overexpressed breast cancer cells were incubated with the indicated doses of Adm for 48 h. Cell viability was assessed with a CCK-8 assay. Protein expression was analyzed by Western blot.  $n = 3$  biological replicates. Paired *t*-test was used for statistical comparison. *P*-value was indicated. The data are presented as means  $\pm$  SD.
- F TOP2A co-IP was performed in five breast cancer patient tumor samples (chemotherapy-sensitive, no. 1-2; chemotherapy-resistant or relapsed, no. 3-5), and the immunoprecipitated fractions were analyzed by Western blot for the indicated proteins.
- G The effects of TOP2A O-GlcNAcylation on tumor xenografts in nude mice. MDA-MB-231 cells with stable TOP2A silencing by shRNA (shTOP2A) were transfected with TOP2A-WT or TOP2A-S1469A expression plasmids. Cells were injected subcutaneously into the axillae of nude mice ( $n = 5$  biological replicates for each group). 1 mg/kg L01 was administered by tail vein injection. Volumes of tumors were monitored with caliper twice a week until 24 days. Paired *t*-test was used for statistical comparison. *P*-value was indicated. The data are presented as means  $\pm$  SD.
- H *In vivo* antitumor performance of Adm in MCF-7/ADR bearing nude mice. MCF-7/ADR cells with stable TOP2A silencing by shRNA (shTOP2A) were transfected with TOP2A-WT or TOP2A-S1469A expression plasmids. Cells were injected subcutaneously into the axillae of nude mice ( $n = 5$  biological replicates for each group). 4 mg/kg Adm and 1 mg/kg L01 was administered. Volumes of tumors were monitored with caliper twice a week until 24 days. Paired *t*-test was used for statistical comparison. *P*-value was indicated. The data are presented as means  $\pm$  SD.
- I Survival rates of MCF-7/ADR bearing mice in different treatment groups within 48 d ( $n = 5$  biological replicates).
- J TOP2A O-GlcNAcylation and the interaction between TOP2A and cell cycle regulators were measured by co-IP in tumor tissues. Cellular O-GlcNAcylation was analyzed by Western blot.
- K IHC staining of Cyclin A2 and p27 in paraffin sections of MDA-MB-231 and MCF-7/ADR tumors. The micrograph scale bar represents 50  $\mu$ m.

explained in two ways. First, our previous research revealed that the synthesis of UDP-GlcNAc through hexosamine biosynthetic pathway is upregulated in cancer cells with chemoresistance (Liu *et al.*, 2018). This accumulation of the pool of sugar substrate might activate OGT and lead to elevated cellular O-GlcNAcylation. In the present study, not only TOP2A O-GlcNAcylation but also global O-GlcNAcylation levels showed significant increases in Adm-resistant cells, while OGT expression levels were comparable in Adm-sensitive and Adm-resistant breast cancer cells, indicating that the upregulation of UDP-GlcNAc might be pivotal in regulating OGT activation and the TOP2A-OGT interaction. In addition, the associations between TOP2A, OGT, and HCFC1 (an auxiliary factor links OGT to chromatin; Daou *et al.*, 2011) were increased in drug-resistant cells and patient samples. This result suggested that HCFC1 may act as an influential partner to recruit OGT to chromatin-bound TOP2A. We also revealed that TOP2A O-GlcNAcylation state regulated the interaction of this enzyme with the cell cycle regulators, suggesting that OGT and HCFC1 might participate in TOP2A-involved chromatin complex assembly. In this sense, changes in the composition of TOP2A complex could also affect the interaction between OGT and TOP2A.

Because Adm is one of the first-line chemotherapeutic drugs in oncotherapy, we used this agent to investigate the impact of TOP2A O-GlcNAcylation on breast cancer resistance. Given one of the primary therapeutic mechanisms of Adm is the stabilization of TOP2Acc (Nitiss, 2009), we provide evidence that O-GlcNAcylation might affect the conformation of TOP2A-DNA complexes and antagonize Adm binding and the formation of TOP2Acc. Although O-GlcNAcylation was found to enhance TOP2A chromatin binding and cleavage in this study, our data suggest that Adm might lose its drug target in resistant cells. Although the deletion of TOP2A O-GlcNAcylation in MCF-7/ADR cells did not fully restore the cell's sensitivity to Adm, suggesting that TOP2A glycosylation is not the only factor that can influence the drug resistance of breast cancer cells, our data still demonstrated that deletion of this PTM could reverse TOP2A O-GlcNAcylation-triggered Adm resistance *in vitro* and *in vivo*. Pharmacological inhibition of OGT was also shown to be as a potential strategy for overcoming Adm resistance in breast cancer-bearing mice, adding support to the idea that TOP2A O-

GlcNAcylation is a promising therapeutic intervention point for drug resistance.

Although TOP2A is a well-known nuclear protein, this enzyme has been reported to diffuse in the cytoplasm under particular circumstances (Turley *et al.*, 1997). Previous studies reported that multiple sequences within the CTD contribute to the robust nucleus localization of TOP2A. The NLS sequence in TOP2A is located between amino acids 1,454–1,497 in the CTD and is important for the proper subcellular localization of TOP2A (Mirski *et al.*, 1997; Wessel *et al.*, 1997). Deletion of TOP2A residues 1,174–1,446, which overlap with the CTD, disrupts nuclear localization and mitotic chromatin association despite retaining the major NLS (Adachi *et al.*, 1997; Linka *et al.*, 2007). Published studies also indicated that the CTD is home to multiple PTM sites (Linka *et al.*, 2007; Kozuki *et al.*, 2017; Hoang *et al.*, 2020), which were found to influence TOP2A catalytic activity, protein stability, and subcellular distribution. Based upon these studies, it is reasonable to infer that S1469 O-GlcNAcylation in NLS could affect the subcellular localization and biochemical functions of this enzyme. The molecular dynamics simulation findings presented here also demonstrated that O-GlcNAcylation at S1469 induced global landscape changes in the auxiliary DNA-TOP2A contact region of the CTD and could assist the formation of an enzymatic reaction complex. This may be the mechanism by which O-GlcNAcylation promotes TOP2A chromatin binding and catalytic activity. Thus, we speculate that the O-GlcNAcylation and other PTMs of particular residues within the CTD, especially in the NLS of TOP2A, could impact TOP2A subcellular localization and then control its ability to bind chromatin, with a rapid exchange between molecules in the chromatin and cytosolic pools apparently governing TOP2A's biological function. The precise mechanisms underlying this regulation remain to be further identified.

Because O-GlcNAcylation can influence other nearby PTMs or even modifications in distant sequences (Ma *et al.*, 2022), we also revealed that O-GlcNAcylation at S1469 enhances the phosphorylation of TOP2A. We cannot rule out the possibility that this change in phosphorylation participates in the O-GlcNAcylation-mediated regulation of TOP2A function. Further research is needed to elucidate the interplay between other PTMs and the O-GlcNAcylation of TOP2A. Nevertheless, our work extends the site-specific function of this modification in regulating the ability of TOP2A to interact with

cell cycle factors, which, in turn, determines downstream cell proliferation-related gene expression and serves as a potential pro-survival mechanism. Although it was reported that the expression of cell cycle inhibitor p27 can be affected by OGT (Caldwell *et al.*, 2010). In the present study, we showed that *O*-GlcNAcylated TOP2A reduced p27 expression, while site-specific *O*-GlcNAcylation deletion (nonglycosylated TOP2A-S1469A) led to opposite result. In patient samples, no clear correlation was found between OGT expression levels and drug sensitivity. Drug-resistant samples with much higher TOP2A *O*-GlcNAcylation levels reduced p27 expression compared with that of the sensitive samples. These data suggested that TOP2A *O*-GlcNAcylation plays a role in regulating p27 expression.

In summary, the evidence provided here shows that elevated *O*-GlcNAcylation impacts TOP2A catalytic activity and breast cancer resistance during chemotherapy. Based on the vital role of TOP2A in cancer progression, we propose that *O*-GlcNAcylation is an important regulator of the cancer cell response stimulated with TOP2A-targeting drugs. Therefore, targeting *O*-GlcNAc signaling may be a potential therapeutic approach for conquering breast cancer chemotherapy resistance.

## Materials and Methods

### Cell culture and reagents

Human breast cancer cell lines (MCF-7, T47D, and MDA-MB-231) and human HEK-293T cells were purchased from Type Culture Collection Cell Bank of the Chinese Academy of Sciences (Shanghai, China) and cultured at 37°C with 5% (vol/vol) CO<sub>2</sub> within 6 months from resuscitation. All the cells were cultured in 90% RPMI-1640 (Gibco) supplemented with 1% penicillin/streptomycin antibiotics (Gibco) and 10% fetal bovine serum (Gibco). Adriamycin (Adm, Sigma) was added to the cell cultures in stepwise increasing concentrations from 0.1 to 10 μM for about 8 months to develop Adm-resistant variant, namely MCF-7/ADR. To maintain the drug resistance, the complete medium supplemented with 1 μM Adm. MCF-7/ADR cells were maintained in complete medium without Adm for 1 week and cells with > 90% viability before subsequent treatments. Cell lines were periodically authenticated by short tandem repeat profiling. Cell lines were routinely checked for Mycoplasma using Mycoplasma PCR Reagent set (Euroclone). LO1 was purchased from BioBioPha Co., Ltd. PugNAc was purchased from Sigma. Other reagents were used as analytic grade or better.

### Plasmids, lentiviral production, and transfection

The sequence coding human full-length (1–1,531) wild-type (WT) human TOP2A and *O*-GlcNAcylation site mutant (Ser1469 → Ala) TOP2A were sequenced and subcloned into lentiviral pLVX-IRES-Neo vector containing an N-terminal HA-tag. Lentiviral shRNA plasmids for TOP2A (#sc-36695-V), OGT (#sc-40780-V) were purchased from Santa Cruz Biotechnology. Scrambled shRNA plasmid (#1864) was purchased from Addgene. Lentiviral vectors were cotransfected with psPAX2 and pMD2.G into HEK-293T cells with Lipofectamine 3000 (Invitrogen). After 48 h, virus supernatant was collected. Cells were cultured in a 6-well plate and incubated in

virus supernatant for 48 h. Stable transfectants were selected with neomycin or puromycin. The sequence coding Flag-tagged human full-length OGT was subcloned into pcDNA3.1 vector. The prokaryotic expression plasmids encoding OGT were a gift from Professor David J. Vocadlo (Simon Fraser University, Canada). The truncated mutants of TOP2A (with 6 × His-tag in C-terminal) were subcloned into pET28a(+) prokaryotic expression vector (transformed into *E. coli* BL21DE3) and pCMV eukaryotic expression vector (transfected into OGT overexpressed HEK293T cells). The primer sequences used in this study are provided in Appendix Table S5.

### Western/lectin blot and co-IP

Total proteins were extracted from cells using western/IP lysis buffer (Beyotime, #P0013) supplemented with protease inhibitor and phosphatase inhibitor cocktail (Roche) at 4°C. Protein concentration of cell lysate was determined by bicinchoninic acid (BCA) protein assay kit (Solarbio, China). Proteins were separated by SDS-PAGE (6–12% gel), followed by Coomassie blue staining or transferred to poly-vinylidene fluoride membrane (Millipore). The membranes were blocked with 5% nonfat milk solution and hybridized with primary antibody at 4°C overnight. After washing, HRP-conjugated secondary antibodies were used for visualization. The primary antibodies used were anti-*O*-GlcNAc RL2 (Abcam, #ab93858, 1:1,000), anti-TOP2A (Proteintech, #24641-1-AP, 1:2,000), anti-OGT (Proteintech, #66823-1-Ig, 1:1,000), anti-HA-tag (CST, # 3724, 1:1,000), anti-GAPDH (CST, #5174, 1:1,000), anti-β-Tubulin (CST, #2128, 1:1,000), anti-Histone 3 (CST, #4499, 1:1,000), anti-HCFC1 (CST, # 69690, 1:1,000), an-P-gp (CST, #13978, 1:1,000); γ-H2AX (CST, #97148, 1:1,000), anti-CDK1 (Proteintech, #67575-1-Ig, 1:2,000), anti-UPF1 (Proteintech, #66898-1-Ig, 1:3,000), anti-PTEN (Proteintech, #60300-1-Ig, 1:1,000), anti-Cyclin A2 (CST, #67955, 1:1,000), anti-Cyclin D1 (CST, #55506, 1:1,000), anti-phospho-Rb (Ser807/811), (CST, # 8516, 1:1,000), anti-p27 (CST, #3686, 1:1,000), anti-phospho-threonine (CST, #9386, 1:1,000), and anti-phospho-serine (Abcam, # ab7851, 1:1,000). Lectin sWGA (Vector Laboratories, #B-1025S, 1:2,000) was used for lectin blotting. The appropriate secondary antibody used were anti-mouse IgG-HRP (CST, # 7076, 1:20,000), anti-rabbit IgG-HRP (CST, #7074, 1:20,000), anti-mouse IgM-HRP (Abcam, #ab97230, 1:20,000), Streptavidin-HRP (CST, #3999, 1:50,000).

For immunoprecipitation (IP) and co-immunoprecipitation (co-IP), each cell lysate was incubated with anti-TOP2A (Proteintech, #24641-1-AP, 1:500), anti-His-tag (Abcam, # ab18184, 1:200) antibodies or anti-HA-magnetic beads (Bimake, #B26102) for 2 h at 4°C, added with protein A/G-magnetic beads (Bimake, #B23201), and rotated at 4°C overnight. Immunoprecipitates were then washed with cold western/IP lysis buffer and then subjected to Western blot analysis. For lectin pull-down assay, each cell lysate was incubated with sWGA-bound agarose beads (Vector Laboratories, #AL-1023S), for 2 h at 4°C. Precipitates were then washed with cold western/IP lysis buffer and then subjected to Western/lectin blot analysis.

### Tumor tissues, microarray, and immunohistochemistry

Tissue microarrays consisting of 145 cases of breast cancer tissue and 15 cases adjacent noncarcinoma tissue were analyzed by

Bioaitech Co., Ltd. Five breast cancer patient tumor samples (chemotherapy-sensitive, no. 1–2; chemotherapy-resistant or relapsed, no. 3–5) were used for co-IP assay. The study was carried out in accordance with The Code of Ethics of the World Medical Association (Declaration of Helsinki). The study and the informed consent obtained from enrolled patients was reviewed and approved by Ethics Committee of the Affiliated Huaian No. 1 People's Hospital of Nanjing Medical University (KY-2022-101-01). Tissue microarrays or paraffin-embedded tissue sections were stained with primary antibody anti-O-GlcNAc RL2 (Abcam, #ab93858, 1:200), anti-TOP2A (Proteintech, #24641-1-AP, 1:200), anti-Cyclin A2 (CST, #67955, 1:200) or anti-p27 (CST, # 3686, 1:100), then probed with HRP-labeled secondary antibody, visualized using diaminobenzidine, stained with hematoxylin, and photographed under microscope. The immunoreactivity was semiquantitatively scored according to the product of categorized percentage of stained cell (0: < 5%, 1, 5–25%, 2: 25–50%, 3: 50–75%, and 4: > 75%) and staining intensity (0: negative, 1: weak, 2: intermediate, and 3: strong), and hence has a range from 0 to 12. An immunoreactivity score below median was considered as low expression, and higher values were considered as high expression. Patients' main characteristics are listed in Appendix Tables S1–S4.

### Cell viability and colony formation assays

Cells at a density of  $\sim 3 \times 10^3$  cells/well were seeded in a 96-well plate and treated with DMSO or Adm with/without L01 or PugNAc for 48 h. The viable cells were determined by Enhanced Cell Counting Kit-8 (Beyotime, #C0041) according to the manufacturer's instructions. Absorbance was read at 450 nm by microplate reader (Biotek).

For colony formation assay,  $1 \times 10^3$  cells were seeded and cultured in 6-well plates for 24 h. Then, the cells were treated with Adm. The medium containing Adm was replaced by the fresh every 3 days. After 15 days, cells were fixed with 4% paraformaldehyde and then stained with crystal violet. The colonies were photographed by a microscope. Colonies with a diameter > 0.5 mm were counted under a microscope.

### In vitro glycosylation assay

Recombinant Flag-tagged OGT purified (Anti-Flag magnetic beads, Bimake, #B26102) from HEK-293T cells and His-tagged truncated variants of TOP2A purified from *E. coli* were mixed in the reaction buffer (2 mM UDP-GlcNAc (Sigma), 50 mM Tris-HCl pH 7.5, 12.5 mM MgCl<sub>2</sub>, 1 mM DTT) in a final volume of 50  $\mu$ L and then incubated at 37°C for 12 h. The reaction product was detected by co-IP. A commercially available human recombinant TOP2A was also used in this study (TopoGEN, #TG2000H-4). For chemoenzymatic labeling of O-GlcNAcylated TOP2A, Click-iT™ O-GlcNAc Enzymatic Labeling System (GalT Y289L) and the Click-iT™ Glycoprotein detection kit (Biotin alkyne) were used according to the manufacturer's instructions (Invitrogen). Briefly, TOP2A was immunoprecipitated using anti-TOP2A antibody. Subsequently, the immunoprecipitated fractions were subjected to O-GlcNAc labeling with GalT1 Y289L using UDP-GalNAz (labeled with azide), followed by a click reaction with alkyne-biotin. The labeled proteins were analyzed using Streptavidin-HRP.

### Mass spectrometry

O-GlcNAcylated TOP2A-C fragment from the *in vitro* glycosylation assay was subjected to SDS-PAGE, and the band corresponding to TOP2A-C was excised from gels. After in-gel trypsin (Promega) digestion according to a standard protocol, peptides were extracted and analyzed by nano-LC system coupled to an Orbitrap Fusion Tribrid spectrometer (Thermo Fisher Scientific). The peptides were loaded into an in-house, 10 cm long analytical column packed with 3 mm C18 resin (Dr. Maisch GmbH, Germany) using mobile phase A (0.1% formic acid). The peptides were then separated by a mobile phase B (ACN/0.1% formic acid) gradient elution with the following three steps: 0–35% for 30 min; 35–80% for 10 min; and 80% for 10 min at a flow rate of 300 nl/min. The mass spectrometer was operated in several modes all in Orbitrap. MS1 spectra were collected in a top-speed data-dependent fashion with a dynamic exclusion of the precursor for 20 s after two repeated activation events. Data-dependent acquisition high-energy collision dissociation (HCD) spectra were collected using 28 NCE. EThcD was performed in the high-pressure linear ion trap with an optimized 50 ms reaction time for ETD ( $2 \times 10^5$  reagent AGC) with 25% supplemental collisional energy. The raw data were searched against the Uniprot human database using Proteome Discoverer 2.2 (Thermo Fisher Scientific). Trypsin was selected as the proteolytic enzyme with a maximum allowance of up to two missed cleavages. Peptides were identified with  $\geq 95\%$  confidence and filtered at a 1% false discovery rate.

### Chromatin complexes isolation

Cells were lysed in hypotonic buffer (10 mM HEPES pH 7.5, 10 mM KCl, 0.1 mM MgCl<sub>2</sub>, 0.4% Igepal CA-630 (vol/vol), protease, and phosphatase inhibitor cocktail (Roche)) at 4°C for 20 min. Chromatin was released from the pellets by treatment with lysis buffer (50 mM HEPES pH 7.5, 50 mM NaCl, 0.05% SDS, 2 mM MgCl<sub>2</sub>, 10% Glycerol, 0.1% Triton X-100, 10 units of Benzonase Nuclease, protease and phosphatase inhibitor cocktail [Roche]) at 4°C overnight. The supernatant was collected as to obtain the chromatin complexes.

### DNA cleavage and decatenation assays

Topoisomerase II cell extracts were prepared by TopII-NucEx Kit (TopoGEN, #TG1050-1) according to the manufacturer's instructions. In brief, transfer the cells to an ice-cold TEMP buffer (10 mM Tris-HCl, pH 7.5, 1 mM EDTA, 4 mM MgCl<sub>2</sub>, 0.5 mM PMSF) and leave the solution on ice for 10 min. To release nuclei, dounce in a tight-fitting glass homogenizer, and pellet nuclei by centrifugation. Resuspend nuclear pellet TEP (same as TEMP but lacking MgCl<sub>2</sub>) and add an equal volume of 1 M NaCl, vortex, and leave on ice for 30 min to extract chromosomal proteins. Centrifuge at 13,000 rpm 20 min and recover the supernatant for topoisomerase II cell extracts. For recombinant TOP2A, TOP2A-WT or TOP2A-S1469A was immunoprecipitated using anti-HA magnetic beads from breast cancer cells and then eluted with 15  $\mu$ g HA peptide (Sigma) in TBS at 4°C. TOP2A protein was quantified by Bradford protein quantification assay (Bio-Rad).

DNA cleavage assays were performed using a negatively supercoiled pBR322 plasmid DNA in 20  $\mu$ L of reaction mixtures (10 mM

Tris-HCl, pH 7.9, 100 mM KCl, 0.1 mM EDTA, 5 mM MgCl<sub>2</sub>, and 2.5% glycerol) at 37°C for 2.5–30 min. Reaction was stopped by adding 2 µL of 10% SDS and 1 µL of 250 mM of EDTA, followed by the addition of 50 µg/ml of proteinase K (Sigma) at 45°C for 30 min. The reaction was then resolved by 1% agarose gel electrophoresis. Double-stranded DNA cleavage was monitored by the conversion of the negatively supercoiled plasmid DNA to linear molecules.

For decatenation of kinetoplast DNA (kDNA), Topoisomerase II Drug Screening Kit (kDNA based) was employed (TopoGEN, #TG1019). In brief, the reactions contained topoisomerase II cell extracts, kDNA, and 1 mM ATP in 20 µL of reaction buffer were incubated for indicated time at 37°C. 1% agarose gel was run, and the cleavage product was observed.

### Band depletion assays

Cells ( $5 \times 10^5$ ) were treated with 1–5 µM Adm for 2 h. Cells were either lysed immediately or incubated in drug-free medium for another 30 min at 37°C (to reverse TOP2Acc) before lysis. Then, the samples were incubated at 90°C for 5 min; gross, mechanical fragmentation of the DNA was achieved by passing the sample into a syringe through a 25-gauge needle. Subsequently, samples were supplemented with MgCl<sub>2</sub> (5 mM), and duplicates were incubated with recombinant endonuclease with DNase/RNase activity (benzonase, 0.4 Units/µl, Sigma) for 30 min at room temperature before Western blot using the anti-TOP2A antibody.

### Flow cytometry and immunofluorescence

Cells were seeded in a 6-well plate and treated with the indicated doses of Adm for 24 h and then fixed in 70% (vol/vol) ethanol overnight at –20°C. After washing with PBS, cells were resuspended with PBS containing RNase A (Sigma) for 30 min at 37°C in the dark and then stained with 5 µL propidium (PI, Sigma) for 30 min at room temperature in the dark. Cells were subsequently analyzed using a flow cytometry (BD).

For immunofluorescence assay, cells on coverslips were fixed in 4% paraformaldehyde for 30 min and permeabilized with 0.1% Triton X-100. Cells were washed with PBS and blocked for 30 min with 5% goat serum. Then, the cells were incubated overnight with primary antibodies against HA-tag at 4°C, followed by incubation with goat anti-rabbit IgG (conjugated with FITC) at room temperature for 2 h. 4',6-diamidino-2-phenylindole (DAPI) was used for nuclear staining. Images were captured under a confocal microscope (Leica).

### TCGA data analysis

Gene expression data and corresponding clinical data for 1,072 patients with breast cancer were obtained from The Cancer Genome Atlas (TCGA) dataset (Chang *et al*, 2013). The Kaplan–Meier survival curves were generated by “survminer” package of R (Version 3.6.3).

### Xenograft mouse model and histopathology

In total, 5–6-week-old female nude mice (Changsheng Biotechnology Co., Ltd, Benxi, China) were used for the establishment of

breast tumor xenografts. All mice were kept in a sterile and comfortable environment and provided food and water *ad libitum*. All animal experimental protocols were approved by the ethics committee of the Xuzhou Medical University (202207S098). All mice were randomly divided into different groups. No blinding was performed during animal experiments. Breast cancer cell suspension containing  $3 \times 10^6$  cells in PBS, followed by injection to the left armpit of the mice ( $n = 5$ /group). Mice were administered OGT inhibitor L01 (1 mg/kg) by tail vein injection every other day, for 20 days. Tumor size was monitored with caliper twice a week until 24 days. For *in vivo* Adm efficacy analysis, the mice were intraperitoneal injected with Adm (4 mg/kg) once a week after the tumor size reached 200 mm<sup>3</sup>. Mice were administered with OGT inhibitor L01 (1 mg/kg) by tail vein injection every other day, for 22 days. Tumor volume was calculated by formula: volume (mm<sup>3</sup>) = width<sup>2</sup> × length × 0.52. For survival analysis, the mice were treated with Adm; general condition, body weight, and survival of the mice were monitored every 2 days. Mice in each cohort were considered to be dead and euthanized either when the tumor volume increased to 1,000 mm<sup>3</sup>, weight loss 20%, scruffy coat, hunched appearance or moribund state. The endpoint of the study was stipulated at 48-day post-tumor cell inoculation. Mice surviving until the end of the efficacy experiment were euthanized. The tumors were then dissected out, fixed, sectioned, and stained with antibody and hematoxylin.

### Molecular simulation

The C-terminal domain (CTD, residue: 1,435–1,522) of TOP2A was taken from the modeling structure of AlphaFold Protein Structure Database (ID: P11388), and totally 1 µs molecular dynamics (MD) simulation was conducted to refine the modeling structure. The DNA sequence from PDB 6ZY5 was used as the template to build a longer double helix structure (extend the sequence from 17 to 34 bp with a repeat) by web server 3DNA (<http://web.x3dna.org/>), and a 500 ns MD simulation was taken the relax and refine the modeling structure.

The modeling structures of CTD and DNA double helix were chosen from the largest cluster of the equilibrium period of MD simulation, respectively. The complex structure of CTD-DNA was calculated with ZDOCK program with S1469 on the interface, and PyRosetta was used for the local refinement of top-5 results from ZDOCK. Three best scored complexes were taken to carry a 1 µs MD simulation for each. From the cluster and PCA analysis results of the MD trajectories, the most typical complex conformation was taken for further study. The glycosylation structure of CTD-S1469 was modeled with GlyCAM server. For the glycosylated and nonglycosylated CTD-DNA complexes, 1 µs MD simulation was conducted in parallel.

All of the MD simulations were performed by Amber20 with Amber14 force field. The structure was solvated in a cubic TIP3P water box with 1 nm distance from the edge, which was neutralized by sodium ions. After four steps of energy minimization, the temperature of the system was gradually heated to 300 K over 100 ps to perform the 10 ns NVT equilibration and 10 ns NPT equilibration subsequently. The production MD simulations at 300 K and 1 atm were carried out with the LINCS algorithm to restrain the hydrogen positions at their equilibrium distances, which allowed the use of an

integration time step of 2 fs. Both energies and coordinates were saved every 10 ps for the postproduction analysis of the MD simulations. All MD simulations were performed on a high-performance computer cluster running the Linux operating system.

### Statistical analyses

Statistical differences were determined using the paired/unpaired Student's *t*-test comparisons (GraphPad Prism 8.0). Survival curves were plotted according to the Kaplan–Meier method. *P*-value < 0.05 was taken as statistically significant. Spearman correlation test was used for correlation analysis. All data were reported as mean ± standard deviation (SD). Detailed *n* values for each panel in the figures are stated in the corresponding legends.

## Data availability

The raw mass spectral data have been deposited to the iProX partner repository (<https://www.iprox.cn/>) under Project ID: PXD041284. The link access to the raw data is: <https://proteomexchange.org/cgi/GetDataset?ID=PX041284>.

**Expanded View** for this article is available [online](#).

### Acknowledgements

This study is supported by the National Natural Science Foundation of China (32171282) and the Fundamental Research Funds for the Central Universities (DUT22YG131). We also thank Professor David J. Vocadlo (Simon Fraser University, Canada) for providing plasmids.

### Author contributions

**Yangzhi Liu:** Data curation; validation; investigation; visualization; writing – original draft. **Kairan Yu:** Data curation; formal analysis; validation; investigation; visualization; writing – original draft. **Keren Zhang:** Resources; formal analysis. **Mingshan Niu:** Resources. **Qiushi Chen:** Resources; software; visualization. **Yajie Liu:** Investigation. **Lingyan Wang:** Investigation. **Nana Zhang:** Investigation. **Wenli Li:** Investigation; writing – original draft. **Xiaomin Zhong:** Resources. **Guohui Li:** Software. **Sijin Wu:** Resources; software; investigation; writing – original draft. **Jianing Zhang:** Resources; writing – review and editing. **Yubo Liu:** Resources; data curation; formal analysis; funding acquisition; investigation; visualization; writing – original draft; writing – review and editing.

### Disclosure and competing interests statement

The authors declare that they have no conflict of interest.

## References

- Adachi N, Miyaike M, Kato S, Kanamaru R, Koyama H, Kikuchi A (1997) Cellular distribution of mammalian DNA topoisomerase II is determined by its catalytically dispensable C-terminal domain. *Nucleic Acids Res* 25: 3135–3142
- Bailly C (2012) Contemporary challenges in the design of topoisomerase II inhibitors for cancer chemotherapy. *Chem Rev* 112: 3611–3640
- Caldwell S, Jackson S, Shahriari K, Lynch T, Sethi G, Walker S, Vosseller K, Reginato M (2010) Nutrient sensor O-GlcNAc transferase regulates breast cancer tumorigenesis through targeting of the oncogenic transcription factor FoxM1. *Oncogene* 29: 2831–2842
- Chang K, Creighton CJ, Davis C, Donehower L, Drummond J, Wheeler D, Ally A, Balasundaram M, Birol I, Butterfield YSN et al (2013) The cancer genome atlas Pan-cancer analysis project. *Nat Genet* 45: 1113–1120
- Chen T, Sun Y, Ji P, Kopetz S, Zhang W (2015) Topoisomerase II $\alpha$  in chromosome instability and personalized cancer therapy. *Oncogene* 34: 4019–4031
- Chikamori K, Grabowski DR, Kinter M, Willard BB, Yadav S, Abersold RH, Bukowski RM, Hickson ID, Andersen AH, Ganapathi R (2003) Phosphorylation of serine 1106 in the catalytic domain of topoisomerase II $\alpha$  regulates enzymatic activity and drug sensitivity. *J Biol Chem* 278: 12696–12702
- Coley HM (2008) Mechanisms and strategies to overcome chemotherapy resistance in metastatic breast cancer. *Cancer Treat Rev* 34: 378–390
- Daou S, Mashtalir N, Hammond-Martel I, Pak H, Yu H, Sui G, Vogel JL, Kristie TM, Affar EB (2011) Crosstalk between O-GlcNAcylation and proteolytic cleavage regulates the host cell factor-1 maturation pathway. *Proc Natl Acad Sci USA* 108: 2747–2752
- Dougherty AC, Hawaz MG, Hoang KG, Trac J, Keck JM, Ayes C, Deweese JE (2021) Exploration of the role of the C-terminal domain of human DNA topoisomerase II $\alpha$  in catalytic activity. *ACS Omega* 6: 25892–25903
- Fielding AB, Concannon M, Darling S, Rusilowicz-Jones EV, Sacco JJ, Prior IA, Clague MJ, Urbé S, Coulson JM (2018) The deubiquitylase USP15 regulates topoisomerase II alpha to maintain genome integrity. *Oncogene* 37: 2326–2342
- Gmeiner WH, van Waardenburg RC (2021) Targeting DNA topoisomerases: past & future. *Cancer Drug Resist* 4: 758
- Guturi KKN, Bohgaki M, Bohgaki T, Srikumar T, Ng D, Kumareswaran R, El Ghamrasni S, Jeon J, Patel P, Eldin MS (2016) RNF168 and USP10 regulate topoisomerase II $\alpha$  function via opposing effects on its ubiquitylation. *Nat Commun* 7: 1–13
- Hevener K, Verstak TA, Lutat KE, Riggsbee DL, Mooney JW (2018) Recent developments in topoisomerase-targeted cancer chemotherapy. *Acta Pharm Sin B* 8: 844–861
- Hoang KG, Menzie RA, Rhoades JH, Fief CA, Deweese JE (2020) Reviewing the modification, interactions, and regulation of the C-terminal domain of topoisomerase II $\alpha$  as a Prospect for future therapeutic targeting. *EC Pharmacol Toxicol* 8: 27–43
- Huang C-C, Tu S-H, Lien H-H, Jeng J-Y, Huang C-S, Huang C-J, Lai L-C, Chuang EY (2013) Concurrent gene signatures for han chinese breast cancers. *PLoS One* 8: e76421
- Jin M, Li J, Hu R, Xu B, Huang G, Huang W, Chen B, He J, Cao Y (2021) Cyclin A2/cyclin-dependent kinase 1-dependent phosphorylation of Top2a is required for S phase entry during retinal development in zebrafish. *J Genet Genomics* 48: 63–74
- Kang X, Song C, Du X, Zhang C, Liu Y, Liang L, He J, Lamb K, Shen WH, Yin Y (2015) PTEN stabilizes TOP2A and regulates the DNA decatenation. *Sci Rep* 5: 1–12
- Kozuki T, Chikamori K, Surleac MD, Micluta MA, Petrescu AJ, Norris EJ, Elson P, Hoeltge GA, Grabowski DR, Porter AC (2017) Roles of the C-terminal domains of topoisomerase II $\alpha$  and topoisomerase II $\beta$  in regulation of the decatenation checkpoint. *Nucleic Acids Res* 45: 5995–6010
- Levi I, Segev Y, Priel E (2012) Type 1 diabetes affects topoisomerase I activity and GlcNAcylation in rat organs: kidney, liver and pancreas. *Glycobiology* 22: 704–713
- Li X, Lewis MT, Huang J, Gutierrez C, Osborne CK, Wu M-F, Hilsenbeck SG, Pavlick A, Zhang X, Chamness GC (2008) Intrinsic resistance of

- tumorigenic breast cancer cells to chemotherapy. *J Natl Cancer Inst* 100: 672–679
- Linka RM, Porter AC, Volkov A, Mielke C, Boege F, Christensen MO (2007) C-terminal regions of topoisomerase II  $\alpha$  and II  $\beta$  determine isoform-specific functioning of the enzymes *in vivo*. *Nucleic Acids Res* 35: 3810–3822
- Liu Y, Ren Y, Cao Y, Huang H, Wu Q, Li W, Wu S, Zhang J (2017) Discovery of a low toxicity O-GlcNAc transferase (OGT) inhibitor by structure-based virtual screening of natural products. *Sci Rep* 7: 1–11
- Liu Y, Cao Y, Pan X, Shi M, Wu Q, Huang T, Jiang H, Li W, Zhang J (2018) O-GlcNAc elevation through activation of the hexosamine biosynthetic pathway enhances cancer cell chemoresistance. *Cell Death Dis* 9: 485
- Liu Y, Chen Q, Zhang N, Zhang K, Dou T, Cao Y, Liu Y, Li K, Hao X, Xie X (2020) Proteomic profiling and genome-wide mapping of O-GlcNAc chromatin-associated proteins reveal an O-GlcNAc-regulated genotoxic stress response. *Nat Commun* 11: 1–17
- Lotz C, Lamour V (2020) The interplay between DNA topoisomerase 2 $\alpha$  post-translational modifications and drug resistance. *Cancer Drug Resist* 3: 149
- Ma J, Wu C, Hart GW (2021) Analytical and biochemical perspectives of protein O-GlcNAcylation. *Chem Rev* 121: 1513–1581
- Ma J, Hou C, Wu C (2022) Demystifying the O-GlcNAc code: a systems view. *Chem Rev* 122: 15822–15864
- Matsumoto Y, Takano H, Fojo T (1997) Cellular adaptation to drug exposure: evolution of the drug-resistant phenotype. *Cancer Res* 57: 5086–5092
- McClendon AK, Osheroff N (2007) DNA topoisomerase II, genotoxicity, and cancer. *Mutat Res* 623: 83–97
- Miller LD, Smeds J, George J, Vega VB, Vergara L, Ploner A, Pawitan Y, Hall P, Klaar S, Liu ET (2005) An expression signature for p53 status in human breast cancer predicts mutation status, transcriptional effects, and patient survival. *Proc Natl Acad Sci USA* 102: 13550–13555
- Mirski SE, Gerlach JH, Cummings HJ, Zirngibl R, Greer PA, Cole SP (1997) Bipartite nuclear localization signals in the C terminus of human topoisomerase II $\alpha$ . *Exp Cell Res* 237: 452–455
- Nitiss JL (2009) Targeting DNA topoisomerase II in cancer chemotherapy. *Nat Rev Cancer* 9: 338–350
- Noach N, Segev Y, Levi I, Segal S, Priel E (2007) Modification of topoisomerase I activity by glucose and by O-GlcNAcylation of the enzyme protein. *Glycobiology* 17: 1357–1364
- Pommier Y, Sun Y, S-yN H, Nitiss JL (2016) Roles of eukaryotic topoisomerases in transcription, replication and genomic stability. *Nat Rev Mol Cell Biol* 17: 703–721
- Pommier Y, Nussenzweig A, Takeda S, Austin C (2022) Human topoisomerases and their roles in genome stability and organization. *Nat Rev Mol Cell Biol* 23: 407–427
- Tewey K, Rowe T, Yang L, Halligan B, Liu L-F (1984) Adriamycin-induced DNA damage mediated by mammalian DNA topoisomerase II. *Science* 226: 466–468
- Turley H, Comley M, Houlbrook S, Nozaki N, Kikuchi A, Hickson I, Gatter K, Harris A (1997) The distribution and expression of the two isoforms of DNA topoisomerase II in normal and neoplastic human tissues. *Br J Cancer* 75: 1340–1346
- Vasan N, Baselga J, Hyman DM (2019) A view on drug resistance in cancer. *Nature* 575: 299–309
- Wessel I, Jensen PB, Falck J, Mirski SE, Cole SP, Sehested M (1997) Loss of amino acids 1490Lys-ser-Lys1492 in the COOH-terminal region of topoisomerase II $\alpha$  in human small cell lung cancer cells selected for resistance to etoposide results in an extranuclear enzyme localization. *Cancer Res* 57: 4451–4454
- Yang X, Qian K (2017) Protein O-GlcNAcylation: emerging mechanisms and functions. *Nat Rev Mol Cell Biol* 18: 452–465
- Zhu C, Zhang L, Zhao S, Dai W, Xu Y, Zhang Y, Zheng H, Sheng W, Xu Y (2021) UPF1 promotes chemoresistance to oxaliplatin through regulation of TOP2A activity and maintenance of stemness in colorectal cancer. *Cell Death Dis* 12: 1–15



## Expanded View Figures

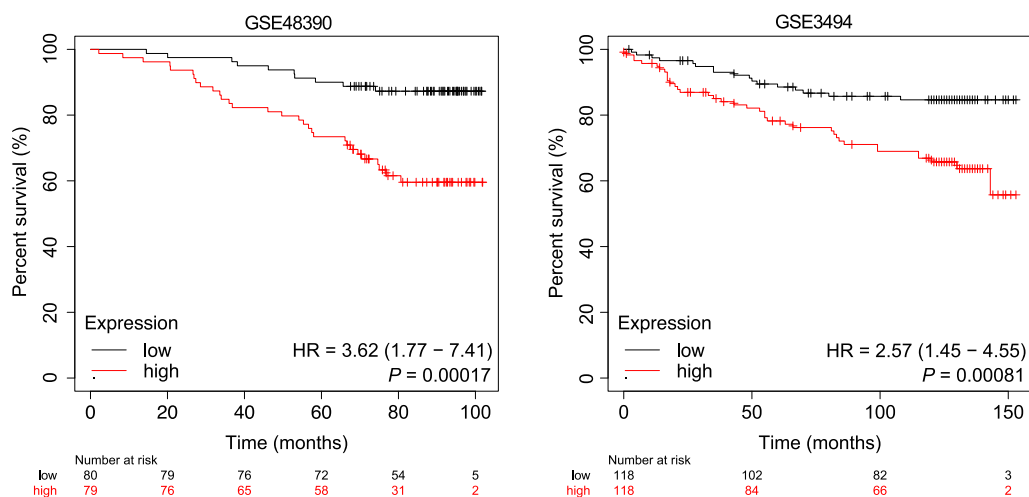


**Figure EV1.** mRNA levels of TOP2A positively correlate with overall survival in human breast cancer tissues.

Datasets used for the survival analysis were obtained from the indicated GEO datasets (GSE48390 and GSE3494). Patients with TOP2A mRNA expression greater than the median are indicated by the red line, and patients with TOP2A mRNA expression below the median are indicated by the black line. HR, hazard ratio. Statistical analysis was performed by the log-rank test. The P-values are indicated (n = 159 biological replicates for GSE48390, n = 236 biological replicates for GSE3494).

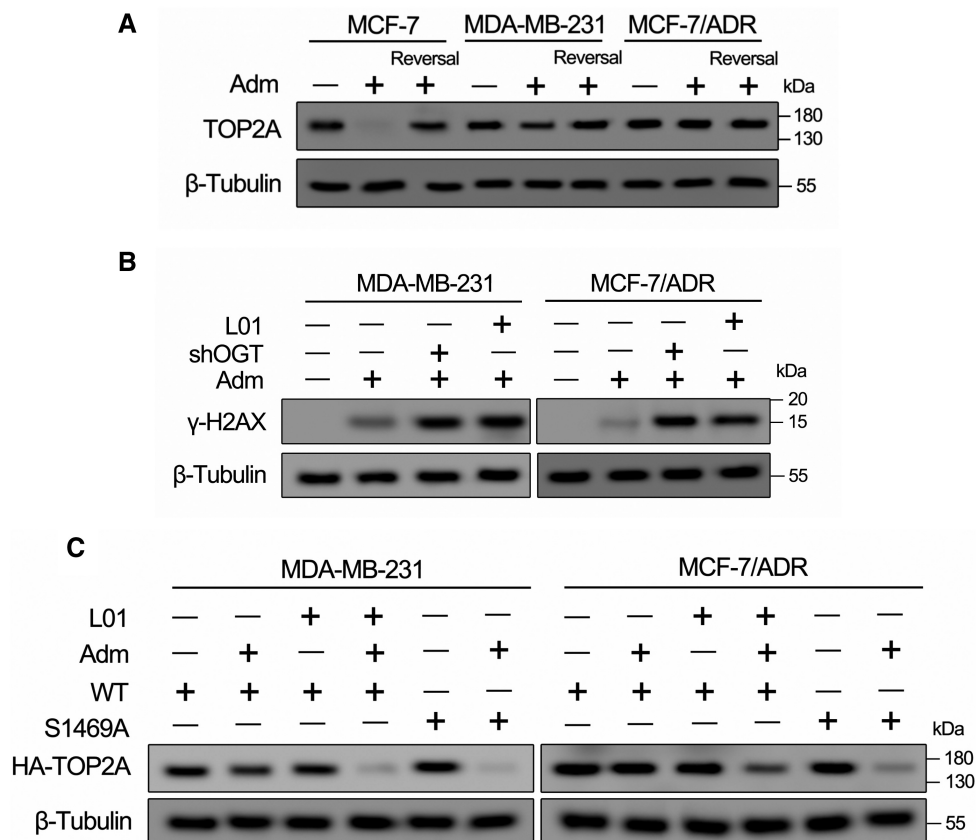


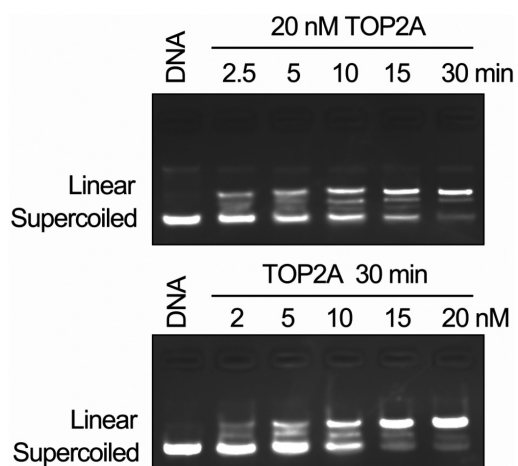
**Figure EV2. Relationship between TOP2Acc and TOP2A O-GlcNAcylation-related Adm resistance.**

A The amount of TOP2Acc in Adm-treated breast cells was measured by a band depletion assay. Indicated cells were treated with Adm (1  $\mu$ M for MCF-7 cells, 5  $\mu$ M for MDA-MB-231 and MCF-7/ADR cells) for 2 h. Cells were lysed either immediately or after reversal of the TOP2Acc (Reversal). Cell lysates were analyzed by Western blot.

B MDA-MB-231 or MCF-7/ADR cells were transfected with OGT shRNA (shOGT) or treated with 50  $\mu$ M L01 for 48 h. The cells were further cultured in the presence or absence of Adm (5  $\mu$ M) for 2 h. Cell lysates were analyzed by Western blotting using anti- $\gamma$ -H2AX antibody.

C Band depletion assays were performed in MDA-MB-231 and MCF-7/ADR cells which stable transfected with HA-tagged TOP2A-WT or TOP2A-S1469A (in the presence or absence of 50  $\mu$ M L01). Breast cancer cells were treated with Adm (5  $\mu$ M) for 2 h. Cell lysates were analyzed by Western blot.

Source data are available online for this figure.



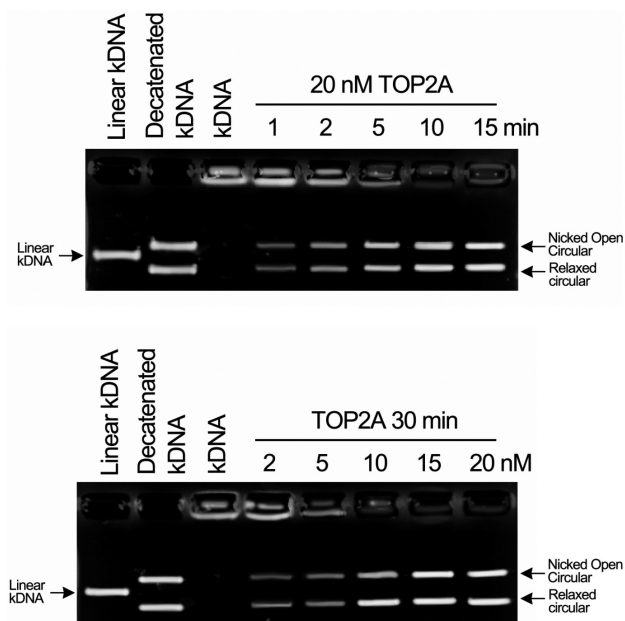


**Figure EV4.** kDNA decatenation assays were measured using the endogenous TOP2A purified from MCF-7/ADR cells.

kDNA was used as the TOP2A substrate. TOP2A could retain catalytic activity *in vitro* and catalyzed kDNA decatenation in a concentration- and time-dependent manner. Linear kDNA was used as the negative control, and decatenated kDNA was used as the positive control. The enzyme concentration and reaction time were indicated.

Source data are available online for this figure.

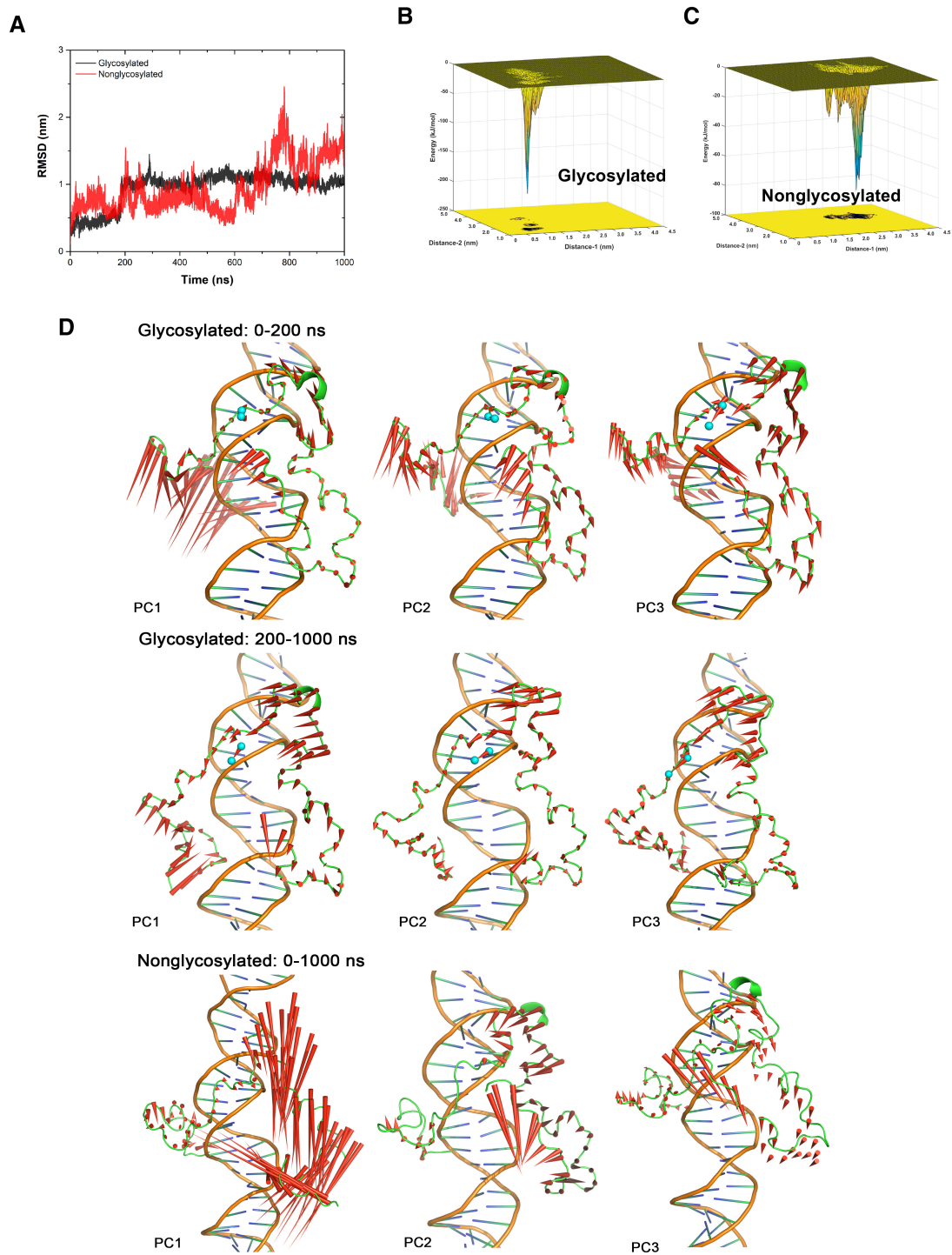


Figure EV5.

**Figure EV5. Molecular simulation of O-GlcNAcylated TOP2A CTD with DNA.**

- A The curves of root-mean-square deviation of CTD C $\alpha$  atoms along with the time traces from the trajectories of glycosylated and nonglycosylated CTD-DNA systems. The fluctuation of glycosylated CTD-DNA system's RMSD was smaller than nonglycosylated system and became steady around 1 nm after 200 ns MD simulation.
- B, C The conformational energy surface of glycosylated (B) and nonglycosylated CTD-DNA systems (C). The energy surface was computed as a function of Distance-1 (center of mass distance between S1469 and 1487-TSK-1489, to indicate the distance between GlcNAc group and adjacent residues) in nm and Distance-2 (center of mass distance between 1441-TKR-1443 and 1510-AKS-1512, to indicate the distance between two terminals of CTD) in nm against the overall 1  $\mu$ s trajectory of each system. Isosurfaces were shown every 1 kJ/mol. There are several small ensemble states and one dominate ensemble state in the energy surface of glycosylated CTD-DNA system that the deepest energy minimum corresponds to Distance-1 about 0.8 nm, Distance-2 about 1.5 nm and energy about  $-225$  kJ/mol. Three consecutive energy minimums in the energy surface of nonglycosylated CTD-DNA system, as shown in Fig 4G, correspond to Distance-1 from 1.5 to 2.5 nm, and Distance-2 around 3.3 nm with energy worse than  $-90$  kJ/mol. This result indicated that glycosylated S1469 enables a tighter conformation ensemble and significantly stabilizes the association between CTD and DNA. Distance-1: center of mass distance between S1469 and 1487-TSK-1489. Distance-2: center of mass distance between 1441-TKR-1443 and 1510-AKS-1512.
- D The difference in protein motion between the first 200 ns and the rest 800 ns simulation of glycosylated CTD-DNA system was obvious from the PCA analysis. The protein is quite dynamic, especially the N-terminal of CTD in the first 200 ns simulation. The interaction network around the glycosylation S1469 (the GlcNAc group shown as cyan sphere) gave the N-terminal loop (residue 1,435–1,450) enough time to close and enter the major groove of DNA that polar and charged sidechain residues (K1439, 1441-TKRD-1444) in this loop could make strong interactions with DNA. The protein dynamics were more stable in the rest 800 ns trajectory. In contrast, the movement in nonglycosylated system was enormous and inhomogeneous in different regions. The residues around S1469 performed strong tendency to move away from DNA, which was unbeneficial for the stable interaction.

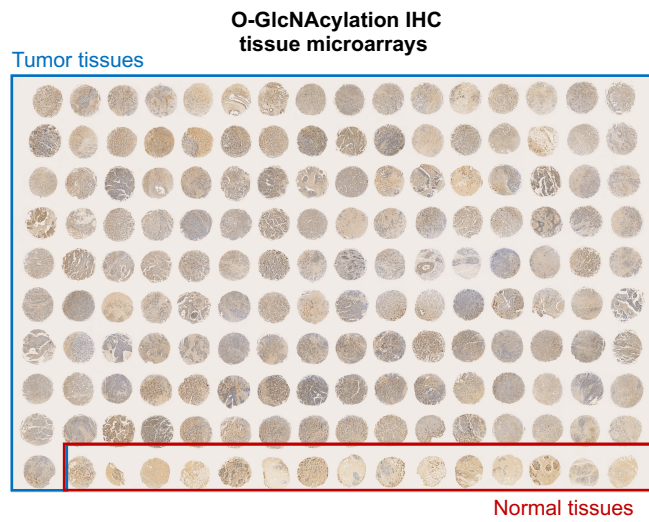
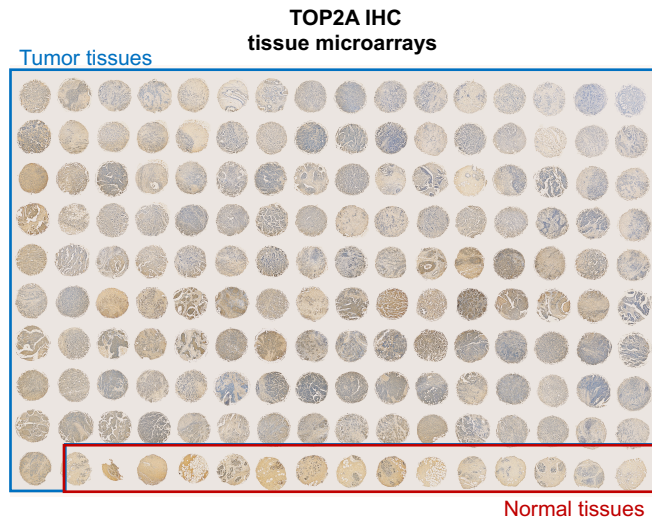
Source data are available online for this figure.

## Appendix

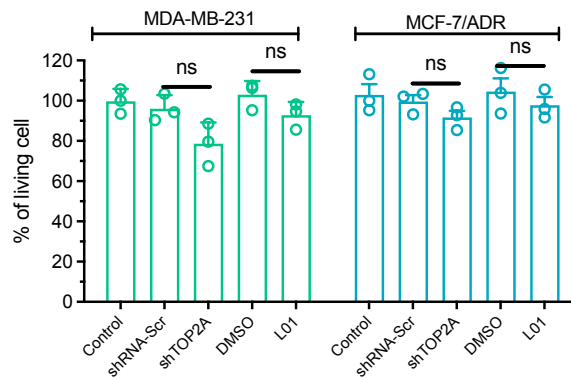
### ***O*-GlcNAcylation promotes topoisomerase II $\alpha$ catalytic activity in breast cancer chemoresistance**

#### Table of content

Content	Page
Appendix Figure S1	2
Appendix Figure S2	3
Appendix Figure S3	4
Appendix Figure S4	5
Appendix Figure S5	6
Appendix Table S1	7
Appendix Table S2	8
Appendix Table S3	10
Appendix Table S4	12

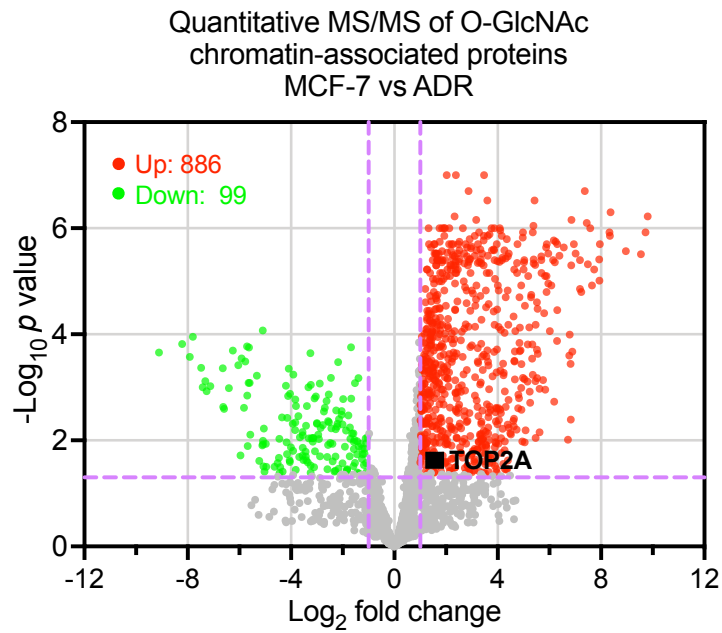


**Appendix Figure S1** Layout and IHC staining of TOP2A and cellular O-GlcNAcylation on a tissue microarray containing 145 breast tumor and 15 adjacent samples.

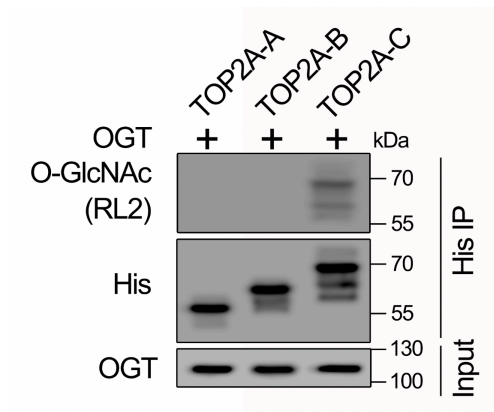


**Appendix Figure S2** MDA-MB-231 and MCF-7/ADR cells were transfected with scrambled shRNA (shRNA-Scr) or TOP2A shRNA (shTOP2A) for 48 h. Or the cells were treated with 50  $\mu$ M L01 for 48 h. The cell viability was assessed through a CCK-8 assay. Protein expression were shown in Figure 2D and E. OGT inhibition itself or TOP2A shRNA transfection itself did not have significant impact on the cell viability in MDA-MB-231 and MCF-7/ADR cells.  $n = 3$  biologically replicates. Unpaired t-test was used for statistical comparison.  $p$  value was indicted.

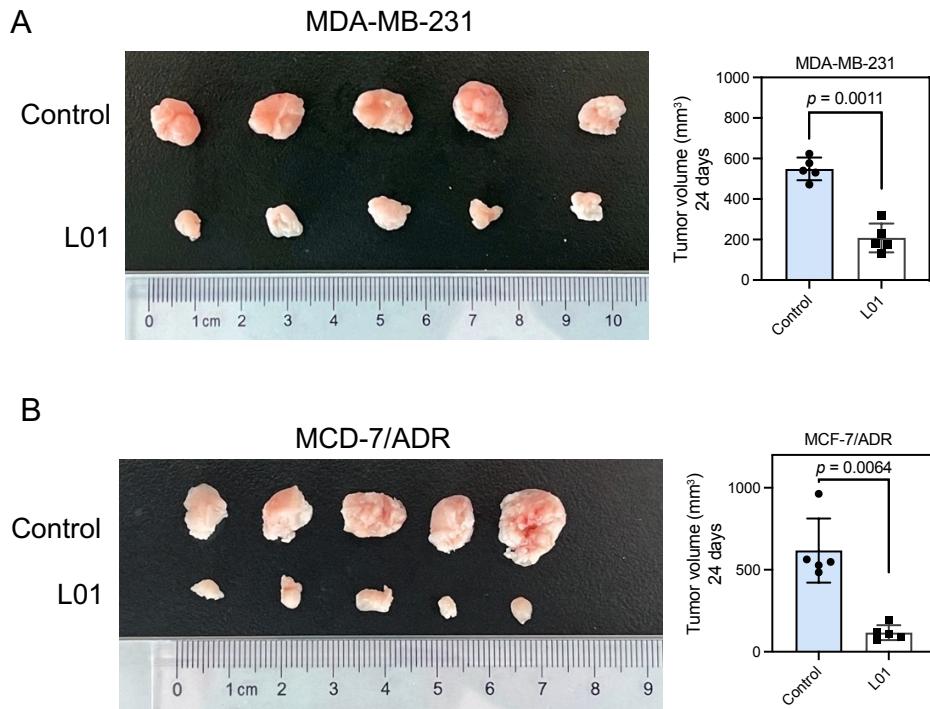




**Appendix Figure S3** TOP2A was previously reported to be a O-GlcNAcylated chromatin-associated protein (*Liu Y, Chen Q, Zhang N, et al. Proteomic profiling and genome-wide mapping of O-GlcNAc chromatin-associated proteins reveal an O-GlcNAc-regulated genotoxic stress response[J]. Nature communications, 2020, 11, 5898*). Volcano plot of label-free relative quantitative proteomics data of O-GlcNAc chromatin-associated proteins in MCF-7 and MCF-7/ADR cells (n = 9 biologically replicates, unpaired t-test). TOP2A was labelled.



**Appendix Figure S4** His-tagged TOP2A-A, -B and -C expression plasmids were transfected with the OGT expression plasmid in HEK-293T cells. After 48 h, His-tag IP was performed, and the immunoprecipitated fractions were analyzed by Western blot for the indicated proteins.



**Appendix Figure S5** The effects of L01 on tumor xenografts in nude mice. (A) MDA-MB-231 cells were injected subcutaneously into the axillae of nude mice ( $n = 5$  for each group). 1 mg/kg L01 was administrated by tail vein injection every other day for 22 days. Control group was treated with DMSO. Volumes of tumors were monitored with caliper twice a week until 24 days. Unpaired t-test was used for statistical comparison.  $p$  value was indicted. (B) MCF-7/ADR cells were injected subcutaneously into the axillae of nude mice ( $n = 5$  for each group). 4 mg/kg Adm and 1 mg/kg L01 was administrated by tail vein injection. Control group was treated with DMSO. Volumes of tumors were monitored with caliper twice a week until 24 days. Unpaired t-test was used for statistical comparison.  $p$  value was indicted.

### Appendix Table S1

The relationship between *TOP2A* mRNA expression and clinicopathological factors in 1072 TCGA breast cancer patients (female).

Variables	No. of patients	TOP2A		Chi-Square	<i>p</i> value
		low	high		
<b>Age</b>					
< 50	292	139	153	0.9225	0.3368
≥ 50	780	397	383		
<b>Stage</b>					
I	188	115	73	11.38	0.0007***
II + III + IV + X	884	421	463		
<b>T classification</b>					
T1	278	168	110	16.34	< 0.0001****
T2 + T3 + T4	794	368	426		
<b>N classification</b>					
NX + N0	523	265	258	0.1829	0.6689
N1 + N2 + N3	549	271	278		

The cutoff for high and low TOP2A expression were  $\geq$  median or  $<$  median, \*\*\* $p < 0.001$ , \*\*\*\* $p < 0.0001$

**Appendix Table S2**

The relationship between TOP2A protein expression and clinicopathological factors in 145 breast tumor samples on a tissue microarray.

Variables	No. of patients (female)	TOP2A		Chi-Square	<i>p</i> value
		low	high		
<b>Age</b>					
< 50	70	30	40	0.6109	0.4344
≥ 50	75	37	38		
<b>Grade</b>					
1	31	20	11	5.318	0.0211*
2 + 3	114	47	67		
<b>Stage</b>					
0 + I	10	6	4	0.3341	0.5633
II + III	135	61	74		
<b>T classification</b>					
Tis + T1 + T2	93	50	43	5.957	0.0147*
T3 + T4	52	17	35		
<b>N classification</b>					
N0 + N1	119	56	63	0.1938	0.6598
N2 + N3	26	11	15		
<b>Lymph node metastasis</b>					
No	96	50	46	3.947	0.047*
Yes	49	17	32		
<b>PR</b>					
Negative	107	46	61	1.699	0.1924
Positive	38	21	17		
<b>ER</b>					
Negative	110	52	58	0.2083	0.6481

Positive	35	15	20		
HER2					
Negative	65	33	32	0.9866	0.3206
Positive	80	34	46		

High group: IHC score  $\geq 4$  (median score), low group: IHC score  $< 3$ ,  $*p < 0.05$ .

**Appendix Table S3**

The relationship between cellular O-GlcNAcylation expression and clinicopathological factors in 145 breast tumor samples on a tissue microarray.

Variables	No. of patients (female)	O-GlcNAc		Chi-Square	<i>p</i> value
		low	high		
<b>Age</b>					
< 50	70	32	38	0.002119	0.9633
≥ 50	75	34	41		
<b>Grade</b>					
1	31	19	12	3.956	0.0467*
2 + 3	114	47	67		
<b>Stage</b>					
0 + I	10	6	4	0.3895	0.5326
II + III	135	60	75		
<b>T classification</b>					
Tis + T1 + T2	93	48	45	3.886	0.0487*
T3 + T4	52	18	34		
<b>N classification</b>					
N0 + N1	119	62	57	11.6	0.0007***
N2 + N3	26	4	22		
<b>Lymph node metastasis</b>					
No	96	51	45	6.63	0.01*
Yes	49	15	34		
<b>PR</b>					
Negative	107	43	64	4.678	0.0306*
Positive	38	23	15		
<b>ER</b>					
Negative	110	47	63	1.43	0.2317

Positive	35	19	16		
HER2					
Negative	65	29	36	0.03864	0.8442
Positive	80	37	43		

High group: IHC score  $\geq 3$  (median score), low group: IHC score  $< 3$ , \* $p < 0.05$ , \*\*\* $p < 0.001$ .



### Appendix Table S4

Clinical characteristics of breast cancer patient samples.

Patient no.	Gender	Age	Grade	Stage	ER	PR	HER2	Chemotherapy-resistant /relapsed
1#	Female	67	2	II	Positive	Positive	Positive	No
2#	Female	52	2	II	Negative	Negative	Positive	No
3#	Female	44	3	III	Negative	Negative	Positive	Yes
4#	Female	48	3	III	Negative	Negative	Negative	Yes
5#	Female	58	3	III	Positive	Positive	Positive	Yes

**Appendix Table S5**

Full-length human wild type and O-GlcNAcylation site mutants TOP2A	Forward	Reverse
Subclone into pLVX-IRES-Neo vector	TTCCTCGAGGCCACCAT GTACCCATACGATGTTCC AGATTACG	ATCCGCGGCCGCTTA AAACAGATCATCTTC ATCTGAC
<i>O</i> -GlcNAcylation site mutant (Ser1469 → Ala) TOP2A	GAATCGCCGCAAAGG AAGCCAGCAACTTCTGA TGATTCTGACTC	GAGTCAGAATCATCA GAAGTTGCTGGCTTC CTTTTGC GGCGATTC
Truncated TOP2A-A	Forward	Reverse
Subclone into pET28a(+) vector	TTCGAGCTCATGGAAGT GTCACCATTGCAG	CTTGTCGACAATACC ACAGCCAATGGCAG
Subclone into pCMV vector	CGGGTCGACATGGAAGT GTCACCATTGCAG	CTTGGGCCCTCAATG GTGATGGTGATGATG AATACCACAGCCAAT GGCAG
Truncated TOP2A-B	Forward	Reverse
Subclone into pET28a(+) vector	TTCGAGCTCGTAGAAAG CATACTAAACTGGG	CTTGTCGACGGTTGT AGAATTAAGAATAGC TAC
Subclone into pCMV vector	CGGGTCGACATGGTAGA AAGCATACTAAACTGGG	CTTGGGCCCTCAATG GTGATGGTGATGATG GGTTGTAGAATTAAG AATAGCTAC
Truncated TOP2A-C	Forward	Reverse
Subclone into pET28a(+) vector	TTCGAGCTCATTGAAAT CTCAGAGCTTCCC	CTTGTCGACAAACA GATCATCTTCATCTG AC
Subclone into pCMV vector	CGGGTCGACGCCACCAT GATTGAAATCTCAGAGC TCCC	CTTGGGCCCTCAATG GTGATGGTGATGATG AAACAGATCATCTTC ATCTGAC
Flag-tagged human full-length OGT	Forward	Reverse
Subclone into pcDNA3.1 vector	CTTGGTACCATGGCGTC TTCCGTGGGC	AGTGGATCCTCACTT ATCGTCGTCATCCTT GTAATCTGCTGACTC AGTGA CTCAAC